Oncogenic RAS drives rapid onset cellular plasticity and elicits a tumour-promoting neutrophil response at the inception of preneoplastic development

Abigail M. Elliot[1a], Isabel Ribeiro Bravo[1b], Jeanette Astorga Johansson[1c], Esme Hutton[1c], Richard Cunningham[1c], Henna Myllymäki [1c], Kai Yee Chang[1], Mariana Beltran[1], Ross Dobie[1], Phil Elks[3], Carsten Gram Hansen[1], Neil Henderson[1], Yi Feng[1,2,*]

1. Centre for Inflammation Research, Institute for Regeneration and Repair, The University of Edinburgh, Edinburgh, EH16 4UU, UK
2. Cancer Research UK Scotland Centre, Institute of Genetics and Cancer, University of Edinburgh, Edinburgh EH4 2XR, UK
3. The Bateson Centre, School of Medicine and Population Health, University of Sheffield, Firth Court, Western Bank, Sheffield, S10 2TN, UK.

a) Current address: CRUK Scotland Institute, Glasgow G61 1BD, UK

b) Current address: UCL Institute of Ophthalmology, 11-43 Bath Street, London, EC1V 9EL

c) These authors contributed equally to this work.

* Corresponding author: yi.feng@ed.ac.uk

Abstract

To date, very little is known regarding the earliest cellular and molecular events within the initial preneoplastic cell (PNC) niche that might determine the outcome of PNC development. Here, we combine *in vivo* live imaging and single cell transcriptomics to investigate the immediate cellular and molecular changes that occur in PNCs and responding innate immune cells within the first 24 hours following tumour initiation. We do so using an inducible transgenic zebrafish model of tumour initiation, in which oncogenic HRAS is conditionally expressed within the zebrafish epidermis. We found that, when expressed within basal keratinocytes, oncogenic HRAS was sufficient to drive several cancer hallmarks in nascent PNCs and their niche. Within 8 hours of oncogenic HRAS induction, basal keratinocytes began to dedifferentiate, followed by a bifurcation in PNC fate towards either a cellular state characterised by partial Epithelial-Mesenchymal-Transition (pEMT) and cancer stem cell features or a more differentiated cell state resembling suprabasal keratinocytes. By directly integrating data from PNCs and human SCC patients we show that both of these PNC states likely persist with established tumours, whilst the pEMT state corresponded with a more aggressive phenotype. Strikingly, markers of the PNC subpopulation that underwent pEMT correlated with poor prognosis in multiple human cancer types in the TCGA database. In addition, the pEMT PNC subpopulation expressed higher levels of cytokines that modulate neutrophil development and function, suggesting a major role for these cells in governing pro-tumour neutrophil responses. Indeed, we found that granulopoiesis was altered within PNC-bearing larvae, with a large proportion of neutrophils switching to an Arginase 2 positive phenotype that functioned to promote PNC

proliferation. Similar to tumour associated neutrophils in the mammalian system, the cxcr1/2 – Il8 axis is involved in mediating the PNC-promoting function of neutrophils in our model. Thus, oncogenic RAS, when activated in the permissive cellular environment is sufficient to drive enabling cancer hallmarks, such as cellular plasticity and inflammation from the inception of the preneoplastic stage of cancer development. Furthermore, these same features may persist to drive malignant progression.

Introduction

Cancer remains the leading cause of death of all diseases despite advances in the development of therapeutics. The most efficient approach to improve patient survival is to detect cancer early, and prevent progression; however, currently 50% of cancers are detected at more advanced stages. There is an urgent need for a better understanding of the basic biology of cancer at the early preneoplastic stage of disease, which would enable the development of better early detection strategies [1] and treatments. Tumours are initiated by clonal expansion of mutated somatic cells that have oncogenic potential, but the immediate subsequent steps that enable mutant cells to progress toward cancer *in vivo* remain unclear [2,3,4]. Mutations in oncogenes or tumour-suppressors genes reported to confer a cell with uncontrolled proliferative capacity and enhanced invasive *properties in vitro*, do not necessarily confer mutant cells with advantages that out-compete normal cells to form a tumour *in vivo*; indeed, it is now clear that a permissive cellular and tissue environment is also necessary for tumour initiation [5, 6, 7]. Recent deep sequencing studies have revealed that a significant proportion of cells in healthy human epithelial tissues carry

cancer-driving mutations that appear to have undergone clonal expansion but do not proceeded to form tumours [8, 9, 10, 11, 12, 13, 14, 15]. Whilst such deep sequencing studies of healthy human tissues have informed us of the accumulation of cells with cancer driver mutations as an ongoing event, very little information can be gleaned from these data regarding the dynamics of mutant clone expansion, progression or regression or their elimination due to changes in host tissue environmental factors *in vivo*. For this, dynamic time-lapse studies in model organisms, preferably translucent model organisms such as *Drosophila* or zebrafish, are necessary [16, 17].

Oncogenic RAS family members are the most prevalent oncogenes in cancer [18]. Although oncogenic RAS mutations are amongst cancer driver mutations detected in selected healthy epithelial tissues, there are tissue that do not typically carry Ras mutant clones. For example, activating KRAS mutations have only been found to be positively selected for in the colorectal epithelium in the case of ulcerative colitis patients [11, 13, 15, 19]. In animal models, clonal expression of oncogenic RAS in various epithelial tissues thas been reported to have variable outcomes; in some cases mutant cells are eliminated by normal neighbouring cells,, whilst in other cases mutant cells are able to undergo proliferation and progression eventually giving rise to tumours [20,21, 22,23]. In zebrafish larval skin, expression of oncogenic RAS has been shown to induce a trophic inflammatory response by host innate immune cells ([24, 25, 26]) and to drive basal invasion at early stages [27]. These observations suggest that the intrinsic cellular state in which oncogenic RAS is activated, and the local tissue microenvironment contribute to the fate of RAS mutant preneoplastic cell fate. Pertinent questions remain, regarding the identity of the enabling features within the initial preneoplastic cell niche that allows RAS mutant cells to expand and thrive.

Here we combine *in vivo* live imaging and single cell RNA sequencing to study the initial cellular and molecular events following HRAS^{G12V} driven preneoplastic cell initiation in the zebrafish basal epidermis. Our data show that HRAS^{G12V} expression causes basal keratinocytes to become transcriptomically distinct compared with control cells within 8 hours post induction and these cells began to show signs of de-differentiation. By contrast, de-differentiation and cell state transition does not occur in HRAS^{G12V} expressing superficial keratinocytes.

Basal-derived PNCs rapidly diversify, form multiple clusters by 24 hours post HRAS^{G12V} induction (hpi). Pseudotime analysis suggested that PNCs diverge along two opposing developmental trajectories, leading either towards suprabasal differentiation or partial Epithelial-Mesenchymal-Transition (EMT). The PNCs that undergo the latter transition potentially harbour cancer stem cell properties. Importantly, following cross-species data integration this subpopulation of PNCs co-clustered with a unique Tumour Specific Keratinocyte (TSK) subpopulation of tumour cells derived from human SCC samples. Such TSKs lead the invasive front in SCC tumour tissues; suggesting that the corresponding PNC cluster may have the potential to drives aggressive phenotypes from the inception of tumour initiation through to late-stage disease. To further test this hypothesis, we queried the expression of the pEMT subpopulation markers within the TCGA database and found a significant association with poor prognosis in many types of human cancer. In parallel twith these cell state transitions, we also demonstrate that HRAS mutant PNCs trigger a systemic tumour promoting neutrophil response within hours of tumour initiation. The cxcr1/2-cxcl8a/b axis is involved in mediating this response, blockade of which partially abrogates

PNC proliferation. This highlights the role of neutrophils in the PNC niche and the speed at which HRAS-driven PNCs begin to alter the host innate immune system to their own benefit.

Results

1. Expression of HRAS^{G12V} in zebrafish basal keratinocytes gives rise to a proliferative tissue microenvironment.

The zebrafish larval epidermis is a simple bilayered epithelium consisting of a superficial periderm and a basal keratinocyte layer [28]. Akin to the mammalian embryonic epidermis, stem cells in the basal layer give rise to all epidermal cell lineages in the adult [29]. In humans, oncogenic HRAS is a driver gene frequently mutated in squamous cell carcinomas [30,31]. Furthermore, HRAS^{G12V} expression leads to the induction of tumourigenesis in mouse and zebrafish cancer models [32,33]. Therefore, to create a model of tumour initiation, we have used the KalTA-ER^{T2}/UAS transgenic system to drive the expression of HRAS^{G12V} (hereafter referred to as HRAS) within the basal epidermis of zebrafish larvae under the control of the *krtt1c19e* promoter (Figure 1 A-D). By 24 hpi HRAS expressing PNCs take on an irregular shape in comparison to the regular polygonal morphology of control keratinocytes expression EGFP-CAAX (CAAX thereafter) (Figure 1 E & F).

Uncontrolled proliferation is a hallmark of cancer [34], however, whether oncogene activation confers an immediate proliferative advantage to PNCs over normal epithelial cells has yet to be described *in vivo*. The inducible nature of the zebrafish epidermis tumour initiation model has allowed us to precisely quantify the rate of PNC proliferation within hours of HRAS expression. We quantified 5-ethynyl-2'-deoxyuridine (EdU) incorporation into newly

synthesised DNA within PNCs compared to control keratinocytes within separate larvae (Figure 1 J). At 18hpi, the percentage of EdU positive PNCs (17.34±1.6 %,) already significantly exceeded that of control keratinocytes (4.01±0.6 %) (Figure 1 K), indicating enhanced proliferation of PNCs. The percentage of EdU positive PNCs continued to increase steadily over time, reaching 43.2±2.5 % at 36hpi. In contrast, the percentage of EdU positive control keratinocytes decreased over the same developmental time span (Figure 1 K). Therefore, HRAS rapidly triggered uncontrolled proliferation within PNCs far greater than the proliferation rate of the growing larval epidermis.

To better understand the tissue dynamics within the PNC-bearing epidermis, we questioned whether the increased proliferation of PNCs might be balanced by the local suppression of proliferation within neighbouring HRAS negative cells. Interestingly, we observed increased EdU+ nuclei immediately surrounding PNCs (Figure 1 L, M). With no additional cell lineage marker, it was not possible to determine the identity of the HRAS negative cells. Nevertheless, EdU positive nuclei were observed in both lateral and apicobasal directions relative to the PNCs, suggesting that enhanced proliferation within the local tissue microenvironment was not restricted to basal keratinocytes.

Oncogene driven hyperproliferation can lead to apoptotic cell death via genomic instability and the DNA damage response [35]. Whilst this can act as a tumour suppressive mechanism, constitutive low level apoptosis is a feature of some solid tumours that may paradoxically exert a pro-tumour influence upon the tumour microenvironment [36]. Therefore, we investigated whether HRAS expression within the epidermis would lead to PNC death. We found that, whilst the majority of PNCs remained TUNEL negative, a higher proportion of PNCs exhibited TUNEL staining at 24 hpi (Figure 1 H) compared with CAAX controls, which

only exhibited minimal TUNEL staining throughout the epidermis. Interestingly, we also observed high levels of TUNEL staining apical to the larger clusters of PNCs, suggesting that the presence of PNCs in the basal epidermis led to the apoptotic cell death of otherwise healthy cells within the overlaying superficial layer (Figure 1 H).

2. Neutrophil recruitment marks an early onset of the inflammatory response to PNCs within 6 hours post HRAS^{G12V} induction followed by macrophage recruitment

We and others have previously shown that RAS expression in various skin cell lineages can induce an inflammatory response in which both neutrophils and macrophages are recruited to RAS expressing cells [25, 37, 38.] However, it is not clear which of these innate immune cells are the first responders, or how early they can first sense PNCs. Taking advantage of the temporal control of HRAS induction, we performed live imaging at 5 hpi, at which time the HRAS positives PNCs can first be detected by confocal microscopy. At this time we clearly observed that neutrophil recruitment toward PNCs had already begun (Figure 2, A, B, Supplementary Movie 1). Recruited neutrophils continuously underwent dynamic transient interactions with PNCs over the duration of 24 hours of time lapse imaging (Figure 2 D D', Supplementary Movie 2). This, taken together with the increase and subsequent maintenance of neutrophil numbers within the PNC-bearing epidermis over time is indicative of chronic inflammation (Figure 2 D, F). Consistent with these observations, we detected upregulation of known neutrophil chemoattractants *ilb*, *il8* and *cxcl18b* in PNC-bearing larvae (Figure 2, E).

Macrophages constitutively patrol the epidermis of healthy zebrafish larvae (Figure 2 G, Supplementary Movie 3). In contrast to neutrophils, macrophage numbers within the PNC-bearing epidermis did not increase above that of controls until much later, at 16 hpi

(Figure 2 J) and preferential interaction with PNCs was not apparent until 24 hpi (Figure 2 H). Upon closer examination of recruited macrophages, we observed that they actively engulfed apoptotic PNC debris (Figure 2 I, Supplementary Movie 5).

3. Syngeneic HRAS-driven PNCs can be separated into phenotypically diverse subsets

The heterogenous cell morphology of PNCs and their dynamic interactions with host myeloid cells prompted us to perform scRNA-seq to analyse the transcriptomic heterogeneity of PNCs and the ensuing myeloid response at 8 and 24hpi (Supplementary Figure 1 A).

Keratinocyte clusters were identified by the expression of keratinocyte markers *krtt1c19e*, *krt5*, and *krt91* (Supplementary Figure 1 B-D). Whilst the majority of these were enriched for basal keratinocyte markers *tp63*, *cldni* and *cldn1*, a small cluster was enriched for superficial markers *krt4*, *cyt1l*, *cldne* and *cldnf* (Supplementary Figure 1 B-D). This is in correspondence with the first characterisation of *krtt1c19e* promoter driven transgenic zebrafish line, in which a small population of superficial keratinocytes was labelled in addition to the entirety of the basal layer [29] . This characteristic later allowed us to reveal a differential response to $HRAS^{G12V}$ expression between basal stem and progenitor cells versus terminally differentiated superficial cells.

Keratinocytes and PNCs were subset for further analysis and the timepoints were integrated using Harmony [39] prior to re-clustering. Control basal keratinocytes from 8hpi and 24hpi clustered together indicating stable cellular states (Figure 3 A), whilst PNCs from each time point were largely separated from each other and from the control basal keratinocytes (Figure 3 A-C). This shows that basal-derived PNCs had already undergone substantial

transcriptomic changes at 8 hours following HRAS^{G12V} expression and continued to change over time, becoming increasingly distinct from normal basal keratinocytes. In contrast, superficial keratinocytes from both CAAX and HRAS larvae clustered together (Figure 3 A, B), indicating that superficial keratinocytes did not similarly undergo a dramatic change in transcriptomic state. Furthermore, pseudobulk differential expression results between CAAX and HRAS populations showed that basal-derived PNCs had 2,851 differentially expressed genes at 24hpi, whilst superficial keratinocytes had 470 (Supplementary Figure 1 G). This suggests that the developmental state of the cell of origin plays an important role in determining the cellular response to oncogenic mutation.

Basal keratinocytes from CAAX larvae formed five clusters (CAAX-1 to CAAX-5), revealing heterogeneity within the population of control basal keratinocytes (Figure 3 C). This pre-existing heterogeneity was lost following HRAS^{G12V} induction, indicated by the presence of a single cluster populated by basal-derived PNCs from the 8 hpi timepoint (PNC-1) (Figure 3 A, C). Subsequently, PNCs from the 24hpi timepoint separated into three distinct clusters (PNC-2 to PNC-4) (Figure 3 A, C).

To elucidate the molecular features underlying the similarities and differences between the basal-derived PNC clusters we inspected cluster-enriched genes obtained by differential expression analysis (Figure 3 D). Cell cycle related genes such as *pcna*, *tubb2b* and *mki67* were upregulated within all PNC clusters (Figure 3 D), which is consistent with the hyperproliferation of PNCs described in Figure 1. Genes enriched within individual clusters of control basal keratinocytes were downregulated within all PNCs clusters, suggesting a departure from normal keratinocyte development (Figure 3 D). Whilst distinct from the control cells, when compared to the other PNC clusters, PNC-1 and PNC-2 possessed only 11

and 10 uniquely enriched genes respectively (Figure 3 D). This suggests that these clusters represent intermediate states, which is supported by the co-expression of CAAX and PNC enriched genes within PNC-1, and the co-expression of PNC-3 and PNC-4 enriched genes within PNC-2 (Figure 3 D). The PNC-3 cluster possessed 811 uniquely enriched genes, including *mmp9* and *mmp13a*, which are known to aid invasion of cancer cells via degradation of extracellular matrix, and numerous genes associated with cancer cell migration via modulation of the actin cytoskeleton, e.g., *tpm4*, *tagln2* and *anxa2,* suggesting enhanced motility of these cells [40, 41, 42]. The PNC-4 cluster expressed 1,017 uniquely enriched genes including *myb*, a key regulator of terminal epidermal keratinocyte differentiation [43] , and *cldna*, a marker of intermediate keratinocytes in adult zebrafish epidermis [43]. Furthermore, PNC-4 expressed high levels of superficial keratinocyte markers, such as *cyt1*, *cytl1*, *cldne*, *cldnb* and *krt17* [43,44], suggesting that subpopulation of PNCs had begun to undergo differentiation to suprabasal fate.

To better understand the developmental relationships between PNC clusters we performed pseudotime analysis using Monocle 3 [45]. The pseudotime trajectory traced a path from PNC-1 (largely composed by 8hpi PNCs) toward a branch point within PNC-2 at which point the trajectory split into two paths towards PNC-3 or -4 (Figure 3 E). Therefore, PNC-2 may represent a nascent, bi-potent PNC state that exists prior to the activation of one of two distinct PNC transcriptional programmes.

Markers of the PNC-3 and PNC-4 clusters were identified using the concordance of multiple differential expression methods to identify genes that were not only specific but all prevalent and highly expressed within the clusters of interest. The topmost marker for

PNC-3 was *lamc2*, which was detected in 94.6% of cells within cluster PNC-3 vs. 6.5 % cells outwith (Figure 3, F). The topmost marker for PNC-4 was *cldna*, which was detected in 94.7% of cells within cluster PNC-4 vs. 6.1% outwith (Figure 3 G). When we used HCR FISH to visualize these markers simultaneously, we confirmed almost mutual exclusive labelling patterns between PNCs (Figure 3, G).

Overall, these results clearly demonstrate that basal keratinocytes possess a permissive cellular state allowing the rapid emergence of transcriptome-wide alterations within 24 hours of $HRAS^{G12V}$ expression. Furthermore, substantial heterogeneity arose within this population of genetically identical PNCs, indicating the divergence towards two highly distinct states.

4. $HRAS^{G12V}$ drives de-differentiation of basal keratinocytes to an embryonic-like state

Developmental plasticity is now recognised as a common contributing factor in tumourigenesis, wherein somatic cells partially de-differentiate, regaining stem or progenitor properties and avoiding terminal differentiation[46]. To explore whether de-differentiation occurs as an early event following tumour initiation, we performed pseudobulk pair wise comparisons between each of the PNC clusters versus control basal keratinocytes. This revealed a shared programme of both up- and downregulated genes common to all of the PNC clusters. In fact the 100 most downregulated genes were co-regulated in PNC-2,3 and 4, and included numerous basal keratinocyte markers such as characteristic keratins and collagens (Figure 4 A). The widespread loss of basal keratinocyte markers strongly suggests that PNCs may undergo a process of de-differentiation, although the expression of *tp63,* the earliest master regulator for basal epidermis fate, was maintained in most PNC clusters (Figure 4 B).

In many aggressive cancers, cells travel backwards along the Waddington landscape and begin to re-express gene programmes reminiscent of embryonic precursors [47, 48, 49, 50]. To determine whether this may occur within HRAS-driven PNCs, we derived gene-sets from published studies of zebrafish embryonic development (see Methods). Indeed, over-representation analysis showed that immature basal epidermal genes were significantly enriched amongst the upregulated genes of all PNC clusters, whereas the mature epidermal gene-set was enriched amongst the downregulated genes of all PNC clusters (Figure 4 C). Furthermore, genes activated by *tp63* were also enriched within the down-regulated genes, despite sustained *tp63* expression (Figure 4 C). However, it is noteworthy that genes negatively regulated by *tp63*, including neuroectoderm genes, were not enriched in any PNC cluster. Therefore, PNCs de-differentiate towards an earlier developmental state but do not trans-differentiate to the neuroectoderm lineage.

Gene Set Enrichment Analysis of GO Biological Processes showed that down-regulated genes were enriched for terms related to differentiation, i.e., "regulation of cell differentiation, "neuromast development", "fin development" and "cell fate commitment" (Figure 4 D). Common up-regulated genes were enriched for "chromatin remodelling" and "histone modification" (Figure 4 D). These included regulators of epidermal development that are known to suppress differentiation and maintain the self-renewal of basal stem cells: *dnmt1*, *uhrf*, *hdac1*, *ezh2*, *actl6a*, *prmt1*, *prmt5* and *bptf* (Figure 4 E)[51, 52, 53]. This strongly suggests that the dedifferentiation of PNCs may be regulated at the epigenetic level.

5. Distinct clusters of PNCs correspond with invasive versus differentiated cells from SCC patient tumours

Having shown that PNC-3 and PNC-4 are two distinct preneoplastic cell states located at the two endpoints of a branched PNC development trajectory, we next sought to determine whether such states were: 1) maintained within established tumours, 2) conserved in human disease. To address both of these questions we performed a comparative analysis with a scRNA-seq data set from human SCC patients published by Ji et al. 2022[16] (Accession number: GSE144240). We used LIGER[54], a method based up non-negative matrix factorization, to directly integrate the PNCs and control basal keratinocytes from the 24hpi timepoint with basal cells derived from 10 SCC patient tumours and matched healthy tissue. The integrated data was then clustered to jointly determine shared cellular states (Figure 5 A). Control basal keratinocytes from zebrafish larvae co-clustered with human basal keratinocytes from the healthy controls, indicating successful data integration (Figure A-C). Moreover, PNC-3 and PNC-4 cells co-clustered with distinct populations of human tumour-derived cells (Figure A-C). This clearly demonstrates the conservation of cellular states between tumour cells from human patients and the PNCs derived from zebrafish basal keratinocytes.

The majority of PNC-4 cells co-clustered with the subset of tumour cells that possessed features indicative of early differentiation towards suprabasal fate (Tumour - Diff) (Figure 5 D, E). Indeed, the PNC-4 cluster uniquely upregulated superficial keratinocyte genes (Figure 5 F). The PNC-3 cells largely co-clustered with a “Tumour Specific Keratinocyte” population (TSK) from human patients (Figure 5D, E). Interestingly, Ji et al[16]. reported that the TSK cells were mainly found at the invasive leading edge of patient tumours and transcriptomic analyses indicated that these cells underwent EMT. Similarly, the PNC-3 cluster was specifically enriched for genes related to EMT and invasion in cancer, such as cell surface

receptors: *cd276* [55], *cd81a* [56], nrp1a/b[57]; and transcriptional regulators: *snai2*, *foxc1b* [58], *klf7b*[59] and *sox11a* [60](Figure 5 G). In addition, genes related to cell migration were also specifically enriched within PNC-3 cells, e.g., components of the arp2/3 complex required for lamellipodia formation, myosins involved in rear contractility, components of migratory signaling pathways and key integrins required for substrate adhesion (Figure 5 G). The upregulation of many of these EMT-related genes was further confirmed by qPCR on FACS sorted PNCs (Figure 5 H).

Morphological changes of PNCs observed by *in vivo* imaging also support the notion that a subpopulation of HRAS-driven PNCs underwent EMT. At 12hpi all PNCs showed a more rounded shape compared with polygonal shaped control keratinocytes (CAAX) and, by 24hpi, 72% of PNC groups were composed of cells with mesenchymal-like morphology, i.e., elongated and/or possessing protrusions resembling lamellipodia (Figure 5 I, J). Time-lapse imaging revealed that these mesenchymal-like PNCs dynamically extended and retracted their protrusions, some of which dissociated from their neighbouring cells and migrated laterally within the plane of the basal epidermis (Figure 5 K, L, Supplementary Movie 4).

These data show that the phenotypic heterogeneity found within tumours can arise within nascent preneoplastic cells possessing a single oncogene, and that these cellular states are robust enough to be conserved across species. Of particular relevance to our conceptual understanding of tumourigenesis is the observation that cells possessing features associated with aggressive malignant tumours, such as EMT, invasion and migration, may exist long before tumour formation.

6. Features of the PNC-3 cluster are associated with cancer stem cells and poor prognosis in multiple cancer types

The similarity between the PNC-3 cluster and the invasive cells at the leading edge of patients tumours prompted us to further investigate the features of the PNC-3 cluster. Firstly, we inspected the expression of canonical EMT markers[61] and found that the PNC-3 cluster did not perfectly adhere to this framework, e.g., certain epithelial markers were upregulated (*cdh1*, *epcam*, *tjp1a*), whilst certain mesenchymal markers were lacking (*cdh2*, *vim*) (Figure 6 A). This suggests that the cells within the PNC-3 cluster underwent only partial EMT (pEMT). It is increasingly acknowledged that EMT programmes vary highly depending upon the cell type, the trigger and the particular EMT-inducing transcription factors [62]. Indeed, *snai2,* was the only well-established EMT transcription factor enriched within the PNC-3 cluster (Figure 6 A) and has frequently been reported to favour pEMT, as opposed to its close family member *snai1* [63, 64].

Interestingly, partial EMT has been associated with cancer stem cells, with hybrid E/M cells possessing greater tumour initiating capacity and phenotypic plasticity than cells at the extremes of the E/M spectrum [65]. Therefore, we inspected the expression of cancer stem cell markers within the PNC-3 cluster [66]. Indeed, cancer stem cell markers *cd44a, thy1* and simple cytokeratins, such as *krt18* [67] were specifically enriched in PNC-3 (Figure 6 B). Furthermore, by HCR FISH staining of *krt18* and PNC-3 marker, *lamc2*, we could detect small collections of *krt18* ^{high} cells amongst *lamc2*$^{+}$ cells (figure 6 C), suggesting that these cells might possess cancer stem cell features.

Akin to normal stem cells, clonal analysis has demonstrated that cancer stem cells undergo only a low rate of proliferation[67]. Cells undergoing pEMT within patient SCC tumours also expressed lower levels of cell cycle related genes than other tumour cells [16]. To infer the relative proliferation rates of the various PNC clusters we utilised the cell cycle scoring

algorithm from Seurat to predict the cell cycle state of each cell. The PNC clusters contained a higher percentage of cells classified as S phase and G2/M phase compared to CAAX controls, as expected for hyperproliferative cells (Figure 6 D, E). However, the PNC-3 cluster had a reduced percentage of proliferating cells in comparison to the other PNC clusters (Figure 6 D, E). Furthermore, the expression of EMT related genes, including CD44, negatively correlated with both S phase and G2/M phase genes (Figure 6 F). This provides further evidence that PNC-3 cells possess properties of cancer stem cells.

If the PNC-3 cells represent the true "tumour initiating" cells responsible for driving cancer progression, we would expect the markers of this cluster to be associated with poor outcomes for cancer patients. To test this hypothesis, we utilized The Cancer Genome Atlas (TCGA) PanCancer dataset. We obtained the human orthologues of the topmost upregulated genes within the PNC-3 cluster and defined patient subgroups according to high/low expression of this gene signature. We found a recurring negative association between patient survival and signature expression for 17 out of the 25 cancer types available. This effect was particularly pronounced in cancer-types known to be driven by RAS mutations (Hazard Ratios: PAAD, 0.16; COAD, 0.54; LUAD, 0.47) (Figure 6 G).

7. Emerging HRAS-driven PNCs trigger changes in granulopoiesis

We and others have shown that neutrophils and macrophages can play a trophic role in promoting PNC growth (reviewed in Elliot et al. 2020)[6]. Using *mpeg* reporter zebrafish [68] to isolate myeloid cells, we identified both macrophages and neutrophils with the scRNA-seq samples (Supplementary Figure 1). However, our differential expression analysis indicated that macrophages underwent minimal transcriptomic changes within 24 hours of PNC induction (Supplementary Figure 2 A - E). Whilst these macrophages mildly upregulated

pro-inflammatory genes, they did not upregulate alternative activation markers frequently expressed by tumour associated macrophages (Supplementary Figure 2 F). Moreover, depleting macrophages lead to no apparent change in PNC growth at 24 hpi (Supplementary Figure 2 G, H). Therefore, we concluded that macrophages do not play an important role following PNC initiation in our model within the time frame of the investigation.

In contrast, re-clustering of neutrophils resulted in the almost complete separation of neutrophils from the two conditions, as early as 8hpi (Figure 7 A), and maintained at 24 hpi (Figure 7 B). Considering that neutrophils were isolated from whole larvae, this shows that the presence of PNCs rapidly triggered a systemic neutrophil response.

Differential expression between the neutrophil clusters derived from CAAX control larvae indicated that the clusters were primarily defined by the stage of neutrophil development. The expression of "Immature" neutrophil genes gradually decreased from C1 through to C4, whilst "Mature" neutrophil genes gradually increased (Figure 7 C). Therefore, these clusters captured a continuum of neutrophil maturation similar to that reported in scRNA-seq studies of mammalian neutrophils [69, 70, 71]. Neutrophil clusters from PNC-bearing larvae also exhibited a continuum of neutrophil maturation from H1 to H4 (Figure 7 C), corresponding numerically to control clusters C1-4 (Figure 7 D). Differential expression analysis between the H1-4 clusters and their maturity-matched control clusters indicated that approx. 200-700 genes were upregulated within each of the H1-4 clusters. This indicates that neutrophils at all developmental stages responded to the presence of PNCs.

Although neutrophils from PNC-bearing larvae spanned the full spectrum of maturation seen in CAAX control larvae, we found many genes related to neutrophil development were differentially expressed between HRAS neutrophil clusters and their CAAX counterparts at

24hpi (Figure 7 C). In the most immature clusters, H1 vs. C1, "Immature" neutrophil genes were downregulated (*lyz*, *cxcr4b*, *myb*) [72, 73, 74], whilst the key transcription factor that governs early granulopoesis, *cebpa* [69], was downregulated in all HRAS neutrophil clusters (Figure 7 C). In addition, the proportion of immature neutrophils was decreased in HRAS vs. CAAX samples at 24hpi, whilst the proportion of mature neutrophils was unaltered (Figure 7 E). This suggests that the presence of PNCs caused acceleration maturation of neutrophils. The expansion of intermediate stage neutrophils might also be due to enhanced proliferation, as we saw that proliferation related genes were upregulated in all neutrophil clusters from PNC larvae with the highest enrichment in the H2 cluster (Figure 7 C). Finally, the master regulator of emergency granulopoiesis, *cebpb* [75], was highly upregulated in the proliferating H2 cluster (Figure 7 C). Taken together, this suggests that an alternative programme of granulopoeisis akin to emergency granulopoiesis may occur within PNC-bearing larvae.

Emergency granulopoiesis typically occurs following a massive loss of neutrophils due to severe inflammatory insult [75]. To assess systemic neutrophil abundance we used the lyz transgenic reporter and performed whole larval imaging (Figure 7 F). Using the mean area of fluorescence as a proxy for neutrophil abundance we found that PNC-bearing larvae had a >2-fold loss of neutrophils compared to control larvae at 24 hpi (Figure 7 G). This is at odds with the high expression of proliferation genes in the HRAS neutrophil clusters, and strongly suggests that large numbers of neutrophils undergo cell death in PNC-bearing larvae. Indeed, the key neutrophil survival factor, *mcl1b*, was downregulated in all HRAS neutrophil clusters (Figure 7 C). The reduction of neutrophils was even more apparent in the CHT

region, although this is likely due to efflux of neutrophils from the CHT (Figure 7 G) which is in agreement with downregulation of *cxcr4b* in all HRAS neutrophil clusters (Figure 7 C) and our previous observations of neutrophil recruitment into the PNC-bearing epidermis (Figure 2 C-F). The mean fluorescence intensity was also significantly reduced within both the CHT and periphery of PNC-bearing larvae (Figure 7 H). This corresponds with the decreased expression of *lyz* and reduced proportion of immature neutrophils described above (Figure 7 C, E). Thus, we have demonstrated that neutrophils in both the periphery and the CHT are affected following PNC induction. Taken together, neutrophil loss alongside increased neutrophil proliferation, accelerated neutrophil maturation, *cebpa* downregulation and *cebpb* upregulation is reminiscent of the onset of the emergency granulopoiesis that occurs in response to neutrophil loss during systemic infections.

8. HRAS-driven PNCs induce a pro-tumour neutrophil response involving the cxcr1/2-cxcl8 axis

Having ascertained that PNCs trigger systemic changes to neutrophils development, we next questioned whether PNCs trigger neutrophil activation. Interestingly, we observed that genes typically expressed in immunosuppressive Tumour Associated Neutrophils, *arg2* and *ptges3b* [76, 77], were upregulated in the majority of HRAS neutrophils clusters as early as 8hpi (Figure 8 A). Conversely, key markers of classical pro-inflammatory neutrophil responses such as *il1b* were downregulated in the majority of HRAS neutrophil clusters and *cybb/nox2* was not differentially expressed (Figure 8 A). We also detected cytokines that are known to drive tumour associated neutrophil development within the PNCs (such as *tgfb*, *csf3b* and *il1b*) [78], [76], [79], which were most highly expressed within PNC-3 cluster (Figure 8 B). The

alternative activation state of tumour associated neutrophils may arise rapidly following tumour intiation, triggered by PNC-derived signals. Using a newly established *arg2* reporter fish [80], we confirmed the presence of *arg2* positive neutrophils within the epidermis of PNC-bearing larvae, in close contact with PNCs (Figure 8 D, F). We also observed a significantly increased proportion of *arg2* positive neutrophils within the CHT of PNC-bearing larvae versus control larvae (Figure C, E), confirming that the programming of neutrophils occurred systemically. These results were supported by the analysis larval digests by flow cytometry: over 50% of total neutrophils from PNC-bearing larvae were *arg2* positive compared to just 3.2% in control larvae (Figure 8 G).

To establish the functional significance of neutrophils upon the nascent PNCs, we used a well-established *gcsf3r* Morpholino to block neutrophil development [26]. This resulted in a substantial decrease in the percentage of EdU positive PNCs at 24 hpi, demonstrating that neutrophils play an important role in promoting PNC proliferation (Figure 8 H). This is in line with a previous study showing that neutrophil depletion lead to reduced numbers of $HRAS^{G12V}$ expressing cells in the zebrafish epidermis [81]. Interrogating the expression of key neutrophil attractants, we found *cxcl8a* and *cxcl8b* were enriched within the PNC-3 and PNC-4 clusters respectively (Figure 8 I). Neutrophils are known to constitutively express receptors for cxcl8, cxcr1 and cxcr2, although only detected cxcr1 was detected by scRNA-seq, probably due to the limitations of transcript capture and low sequencing depth inherent to this method (Figure 8 J). However, this does suggest that *cxcr1* is expressed at a higher level than *cxcr2*. To establish the role of the *cxcr1/2 – cxcl8a/b* axis, we treated PNC-bearing larvae with CXCR1 and CXCR2 inhibitors. To our surprise, this did not reduce the number of neutrophils recruited to the epidermis (data not shown) although, we did

detect a reduction in direct contact between neutrophils and PNCs (Figure 8 K). Notably, we detected reduced EdU incorporation in PNCs following inhibitor treatment, suggesting a decreased proliferation of PNCs (Figure 8 L). Taken together, our data highlight an important role of the CXCL8 - CXCR1/2 axis in mediating neutrophil promotion of preneoplastic growth.

Discussion

Although the initial preneoplastic cell (PNC) developing niche plays a determinant role in promoting successful tumourigenesis, little is known concerning events at the tissue level as well as cellular and molecular events during the earliest stages following PNC initiation. Our study is the first of its kind to investigate cellular and tissue responses to nascent PNCs at the single cell level.

Murine studies have shown that transgenic expression of oncogenic HRAS within the epidermis has heterogenous outcomes varying from benign papillomas to squamous cell carcinomas (SCC), themselves containing transcriptomically heterogenous subpopulations of cancer cells. [32, 67] Yet it is unclear when and how such heterogeneity arises. Our findings demonstrate that cellular heterogeneity occurs at a much earlier stage followiing initiation than previously presumed, within 24 hours of oncogenic HRAS activation. Our scRNA-seq time course and pseudotime analysis suggests dedifferentiation occurs within HRAS expressing basal keratinocytes prior to the emergence of PNC heterogeneity. Dedifferentiation enables the unlocking of cellular plasticity, recognised to be a key cancer hallmark responsible for malignant cancer pathogenesis [46]. Here we found that the intrinsic cellular state of the basal keratinocytes possesses a permissive intracellular state susceptible to the unlocking of phenotypic plasticity in response to oncogenic RAS while the

superficial keratinocytes do not have such a property. At their inception, these basal-derived PNCs dedifferentiate into a state resembling immature embryonic epidermal stem cells and can then transition toward heterogenous cellular states. Future research into the features of such a permissive cellular state will help us to pinpoint the cells of origin regarding tumour initiation, as well as providing targets to develop early detection and cancer prevention strategies.

Significantly, amongst diverse clusters, we find that the PNC-3 cluster underwent pEMT and expresses cancer stem cell markers, suggesting the cells may possess greater potential for tumourigenesis and malignant progression. Consistent with these findings, we found that marker genes of the PNC-3 cluster correlated with poor prognosis in several human cancers in the TCGA database [82], including PAAD, COAD, and LAUD all of which have a high incidence of oncogenic RAS mutations. Moreover, the PNC-3 cluster co-segregated with a tumour specific keratinocyte (TSK) cluster in human SCC patients, that was found at the invasive front, where cancer stem cells might reside[67,83]. Therefore, the PNC-3 cluster could harbour cancer stem cells. In support of this possibility, using HCR RNA in situ we found that a small fraction of *lamc2* (PNC-3 cluster marker) positive PNCs upregulated cancer stem cell marker, *keratin 18*. These observations suggest that cells with cancer stem cell features might emerge very rapidly following the initiating expression of HRAS. Whilst not yet confirmed whether these cells are true cancer stem cells capable of giving rise to the entire community of heterogenous tumour cells, they likely have a high degree of cellular plasticity, and it will be important to determine how these cells are specified and whether such a switch can be blocked. Our future work will generate novel genetic tools to perform lineage tracing so as

to follow the development of these k18^{+} cells and isolate them in order to characterise their tumourigenic potential and molecular features.

A recent study highlighted the cross talk between HRAS mutant skin cancer stem cells with cells within microenvironment during the course of malignant progression[67]. We found that HRAS-driven PNCs actively interacted with the host microenvironment, by altering the rate of proliferation and cell death in the surrounding tissue, and by eliciting both systemic and local myeloid responses. The most striking response occurred within neutrophils , which were programmed toward a tumour promoting phenotype. Interestingly, cytokines known to regulate neutrophil development, recruitment and function were highly expressed by the PNC-3 cluster, further expanding the potential for these cells to drive tumour promotion and progression.

Tumour associated neutrophils are known to promote the formation of metastatic tumours [79]. However, it is unclear whether neutrophils play the same role during primary tumour formation, and what the nature of the initial neutrophils response is at the preneoplastic stage. Our data demonstrate that initiating PNCs are themselves responsible for driving the development of a tumour promoting inflammation by altering neutrophil development. Although we and others have previously shown that neutrophils are recruited to PNCs and promote their growth [25, 6, 37,] it is unexpected that in our model, PNCs induce a systemic neutrophil response and altered neutrophil development. Within 24 hours of HRAS induction, the total number of neutrophils with whole larvae was greatly reduced, suggesting that PNCs release inflammatory mediators at sufficiently high levels to drive activation of neutrophils and accelerate neutrophil death. We also observed compensatory enhanced neutrophil proliferation and upregulation of the key transcription factor for

emergency granulopoiesis, *cebpb*, indicating that an alternative programme of neutrophils development resembling emergency granulopoiesis occured within PNC-bearing larvae. However, the neutrophil activation state(s) in our model were different from infection induced emergency granulopoiesis, in that neutrophil numbers were reduced but never depleted and pro-inflammatory genes were downregulated in neutrophils from PNC-bearing larvae, contrary to infection trained neutrophils. It remains to be determined whether the differences between PNC "trained" neutrophils and bacteria "trained" neutrophils lead them to be functionally distinct. Previously, we have reported that neutrophil-derived PGE2 is one of the trophic factors that promotes PNC growth. Consistent with this finding, we observed upregulation of *ptges3b* in neutrophils from PNC-bearing larvae. We also found that the cxcr1/2-cxcl8a/b (il8a/b) axis was important for mediating the trophic effect of neutrophils upon PNCs. Similarly, the cxcr1/2-il8 axis appears also to be important for tumour promoting neutrophils in another zebrafish tumour initiation model and in multiple mammalian models [37, 24, 84], suggesting a conserved mechanism in mediating tumour promoting neutrophil development and function.

In summary, our work demonstrates that cellular plasticity occurs from the inception of preneoplastic development in a permissive cellular environment. A cellular state characterised by partial EMT and features of cancer stem cells became evident within hours of PNC emergence and these cells might represent true tumour initiating cells. Importantly, HRAS-driven PNCs actively forged a tumour-promoting microenvironment by altering the local tissue and co-opting host cells. Our inducible tumour initiation model is ideal for future studies to elucidate mechanisms governing tumour promotion within the developing preneoplastic niche. The findings presented here, regarding the cellular states of PNCs and

the nature of the initial myeloid response to tumour initiation, provide valuable information for the development of cancer prevention and early detection strategies.

Materials and Methods

Transgenic Zebrafish strains

The zebrafish lines used in this study include Tg(krtt1c19e::KalTA4-ER^{T2}; cmlc2::EGFP)^{ed201} (hereafter K19 Gal4 driver) [81]. Tg(UAS::EGFP-HRAS^{G12V}; cmlc2::EGFP)^{ed203} [81] & Tg(UAS::mCherry-HRAS^{G12V}; cry::CFP)^{ed205} & Tg(UAS::BFP-HRAS^{G12V}; cry::CFP)^{ed209}; (hereafter UAS:HRAS)[11]. Tg(UAS::EGFP-CAAX; cmlc2::EGFP)^{ed204} [81] & Tg(UAS::mCherry-CAAX; cry::CFP)^{ed206} (hereafter UAS:CAAX) [11]; Tg(lysC::NLS-mScarlet)^{ed229} [85]; TgBAC(arg2:EGFP)^{sh571} (hereafter arg2 reporter)[80]

Zebrafish maintenance and breeding

Adult zebrafish were maintained in the Bioresearch & Veterinary Services (BVS) Aquatic facility in the Queen's Medical Research Institute, The University of Edinburgh. Housing conditions were described in the Zebrafish Book (Westerfield, 2000)[86] with 14/10 hours light/dark cycle and water temperature of 28.5 °C. Zebrafish larvae were maintained in petri dishes containing 0.3× Danieau's solution (17.40 mM NaCl, 0.21 mM KCl, 0.12 mM $MgSO_4 \bullet 7H_2O$, 0.18 mM $Ca(NO_3)_2$, 1.5 mM HEPES), in a 28.5 °C incubator. All experiments were conducted with local ethical approval from The University of Edinburgh and in accordance with UK Home Office regulations (Guidance on the Operations of Animals, Scientific Procedures Act, 1986) under the authority of the Project Licence PEE579666.

4-Hydroxy-tamoxifen induction and drug treatment.

PNC inductions were described in details previously[87]. In brief, 0.3× Danieau's solution containing 5 µM 4-Hydroxy-tamoxifen (4-OH-tamoxifen, SIGMA) and 0.5% DMSO was used as induction solution. At 48 hours post-fertilisation (hpf), selection marker positive larvae were transferred to 90 mm petri dishes containing 20 ml 4-OHT induction solution, at 50 larvae per dish. The larvae were then maintained at 28.5 °C in the dark. For drug treatment, larvae with GFP positive skin cells were selected at around 8hpi using fluorescent dissecting microscope and randomly separate into three groups. They were then transferred into fresh induction solution or induction solution containing inhibitors, SB225002 1µM or Reparixin 1µM.

Morpholino knockdown of csf3r

A 1 nl bolus of 1 mM previous validated translation block csf3*r* morpholino (GeneTools, 5'-GAAGCACAAGCGAGACGGATGCCAT-3')[26] was injected into the yolk of each egg using a PV 820 pneumatic picopump. Embryos injected with a 1 nl bolus of 1 mM human β-globin morpholino (GeneTools, 5'-CCTCTTACCTCAGTTACAATTTATA-3') was used as control. Success of the *csf3r* knockdown was validated by fluorescence microscopy to assess the reduction in the number of lysC:NLS-mScarlet^{+} neutrophils.

Zebrafish larval EdU (5-ethynyl-2-deoxyuridine) incorporation and staining

The detailed protocol was published in protocol.io [88]. In brief, 4-OHT induced larvae were selected for positive expression signal at 8hpi, and if required appropriate drugs were added to fresh 4-OHT induction solution for further treatment until a defined time. Then, 2nl of EdU solution (10mM) was injected into the yolk of individual larva and after 2.5 hours, larvae were fixed with 4% PFA for 30 minutes at room temperature. EdU staining was

carried out using the Click-iT Plus Edu Alexa FluorTM 647 Imaging Kit (Thermo Fisher Scientific, C10640) following manufacturer's instructions. In brief, larvae were washed thrice in PBS containing 0.5% Triton X-100 (PBST) for 5 minutes and blocked with PBST containing 3% (w/v) Bovine Serum Albumin (Sigma-Aldrich, Gillingham, UK) for 1 h. This was followed by 30 min incubation with the Click-it Plus reaction cocktail using 250 µl of reaction cocktail per 10 larvae. Following EdU labelling, larvae were transferred to wholemount staining for GFP or HRAS.

TUNEL Labelling

Cell death was assessed using the Click-iT™ Plus TUNEL Assay for In Situ Apoptosis Detection Alexa Fluor™ 647 Imaging Kit (Life Technologies, C10617). Unless otherwise stated, all washes and incubation steps were carried out at room temperature with light shaking (60-65 rpm). Larvae were transferred to 4% PFA and incubated for 2 hours at room temperature. Following 3X5 minutes wash in PBST, larvae were permeabilized with 10 µg/mL Proteinase K in PBST for 3 minutes. Larvae were then immediately rinsed twice in PBST and re-fixed for 20 min at room temperature. After 4 X 5 min washes with PBST, larvae were incubated in TdT reaction buffer for 10 min at 37°C, then transferred to TdT reaction mix (TdT reaction buffer, EdUTP, TdT enzyme), made as per manufacturer's instructions, and incubated for 1h at 37°C. Larvae were then incubation in PBST containing 3% (w/v) Bovine Serum Albumin blocking solution for 1 hour at room temperature, then transferred to the Click-it Plus TUNEL reaction cocktail (1x Click-iT Plus TUNEL reaction buffer, copper protectant, Alexa Fluor 647 picolyl azide dye, Click-iT Plus TUNEL reaction buffer additive), made as per manufacturer's instructions, and incubated for 30 min at 37°C in dark. Post staining larvae were transferred to wholemount immunostaining for GFP or HRAS.

Wholemount fluorescent immunostaining

Post EdU or TUNEL stained larvae were washed thrice with PBST for 5 min and re-blocked with PBST containing 5% (v/v) Goat Serum (Sigma-Aldrich, Gillingham, UK) for 2 h. EGFP immunostaining was performed with rabbit monoclonal anti-GFP antibody (1:200; cat. 2956, Cell Signaling Technology, London, UK) and Alexa Fluor 488 Goat anti-Rabbit secondary antibody (1:250; Invitrogen A-11008, Fisher Scientific, Loughborough, UK) or mouse monoclonal antihuman hRAS antibody (1:200; BD Biosciences, 610001) and goat anti-mouse IgG (H+L) Alexa Fluor 488 (1:250; Invitrogen A-11001). Stained larvae were stored at 4 °C in a glycerol based anti-fadent mountant (AF1, CitiFluor, Hatfield, PA, USA) until mounted for imaging.

HCR RNA fluorescence in situ hybridisation (HCR RNA-FISH)

Zebrafish larvae were fixed overnight in in 4% formaldehyde at 4 °C. The embryos were dehydrated in a sequence of 25%, 50%, 75%, and 100% methanol and stored in -20 °C for at least 2h. The HCR *in-situ* probes for *lamc2* (XM_003197884.5), *cldna* (NM_131762.2) and keratin 18 were ordered from Molecular Instruments and the HCR protocol was adapted from the manufacturer's instructions. In brief, larvae were rehydrated following a methanol sequence of 75%, 50%, 25% and 1XPBST, followed by proteinase K (PK) treatment at 8µg/ml for 15 min at room temperature. PK treated larvae were re-fixed in 4% PFA for 20 minutes room temperature before wash in PBST. Larvae were then transferred to 250µl pre-hybridization buffer for 37 °C for 30 minutes, then larvae were transferred into 250µl fresh hybridization buffer contain 16nM each probes overnight at 37 °C. Post hybridization, larvae were washed in 250µl probe washing buffer 4 X 15 minutes at 37 °C, followed by 2 x washing in 500µl 5X SSC at room temperature. Larvae were then transferred into 250µl

amplification buffer for 1h at room temperature followed by transferring into 250µl amplification buffer containing snap cooled H1 and H2 hairpin pairs (30nM) and kept in the dark for >12 hours at room temperature. Next day hair-pin solution removed and thoroughly washed with 500ul 5XSSC at room temperature and sample be stored in AF anti-fading agent at 4 °C before imaging).

Total RNA extraction from whole larvae

Multiple larvae with the desired phenotype (40-50 larvae per group) were transferred to 500 µL TRIzol reagent (Invitrogen) to preserve RNA integrity. Following an over-night at -80°C, samples were thawed and homogenized by repeatedly passing through a 23-gauge needle (BD Microlance) with the help of a 1 mL syringe (BD Plastipak) and vigorous vortexing. Total RNA was isolated with chloroform extraction followed by isopropanol precipitation. After a 2-hour incubation at -20°C to allow full RNA precipitation, RNA was pelleted by centrifugation at 4 °C, 14000rpm for 15 minutes. Pellet was then washed with 70% Ethanol and re-centrifuged with the same parameters. After removal of 70% Ethanol, pellet was air-dried for 5 minutes and resuspended in Nuclease-Free Water (Invitrogen, AM9930).

cDNA synthesis from total RNA

cDNA synthesis was achieved using the iScript™ Advanced cDNA synthesis Kit for RT-qPCR (Bio Rad, 1725037). As per manufacturer's instructions, 4 µL 5x iScript Advanced Reaction Mix and 1 µL iScript Advanced Reverse Transcriptase were added to 15 µL isolated RNA. Resulting reaction mixture was incubated at 46°C for 20 minutes and then at 95°C for 1

minute, in a Mastercycler Nexus Gradient GSX1 Thermal Cycler (Eppendorf). cDNA was stored at -20°C.

Generation of single cell suspension from zebrafish larvae

Detailed protocol can be found in protocol.io. In brief, dissociation Solution contains Media A (HBSS (-Mg, -Ca, + phenol red) (Gibco, 11530476]), 1M HEPES (Sigma Aldrich, H3375), 25mM D-Glucose (Sigma Aldrich, G8644), 2% Sterile Goat Serum (Life Technologies, 16210064), supplemented with 2.5 mg/ml Collagenase IV (Life Technologies, 17104019). 50 larvae were immersed in 2ml Dissociation Solution per well in a 12 well plate and disrupted by repeated rapid pipetting with a P1000 Gilson pipette for 30 seconds, followed by 5-minute incubation at 28.5 °C, with shaking at 100 rpm. After 3 rounds of rapid pipetting + incubation, digests from 3 wells were pooled into a Falcon tube. The digests were then centrifuged at 4°C for 5 minutes at 500g, the pellet was then resuspended in 500µl of fresh Media A.

Flow Assisted Cell Sorting of keratinocytes, PNCs and myeloid cells

Larval digests were passed through a 40µM mesh filter into a FACS tube and DAPI was added to the media (1:1000). Live single cells were selected on the basis of side scatter, forward scatter and DAPI staining. Keratinocytes and PNCs were selected by the fluorescence of the mCherry-CAAX and mCherry-HRAS^{G12V} transgenes respectively. Myeloid cells were selected by fluorescence from the mpeg1.1:EGFP reporter. Autofluorescent cells were excluded by gating out cells with fluorescence in both B 525/50 and B 695/40 filters. Both mCherry and EGFP positive cells were sorted into a single 1.5ml Eppendorf containing 50µl of Media A supplemented with 10% Sterile Goat Serum at 4°C.

cDNA synthesis from FACS sorted cells following the adapted Smart-seq2 protocol

FACS sorted HRAS or CAAX populations were collected directly into Eppendorf tubes containing 4 µL 0.2% Triton X and RNAase inhibitor (Thermo Fisher Scientific) at 1,000 cells per tube. The smart-seq2 protocol was used to prepare the samples for cDNA synthesis (Picelli et al., 2014)[89]. In brief, cDNA quality was assessed using a LabChip GX machine.

Quantitative PCR

Gene expression levels were measured on a LightCycler 96 system using the LightCycler 480 SYBR Green I Master mix (Roche). The primer sequences were the following: *arpc5a* forward 5'-AGTGCTGAAGAATCCACCCA-3' and reverse 5'-ATCGCTAGCCTTGAAAGAGC-3'; *snail2* forward 5'-GACGCACAGAGTCGGAAATC-3' and reverse 5'-TCTAATGTGTCCCTGCAGCA-3'; *mmp9* forward 5'-ACCCTCGATTCACTGATGCA-3' and reverse 5'-CTCCAGTAGAAGCTCTCCCG-3'; *itgb1b* forward 5'-TGCGACAACTTTAACTGCGA-3' and reverse 5'-TGCCGGTGTAGTTAGCATCA-3', *itga5* forward 5'-TGTGTAATGTTGGCCTGTTGG-3' and reverse 5'-TGTAACTAGCATGGCACTCC-3'; *itga3* forward 5'-TGTGATCAGCCAGCGAGA-3' and reverse 5'-CATCTGAAGGTTGCTCTCGC-3'. *cnppd1* forward 5'-TGGCGATTTGTTTGACGAGC-3' and reverse 5'-TCACTCTCTCTGACCACTGC was used as the normaliser gene.

10X single cell RNA-sequencing

For each sample, 60,000 cells were sorted by FACS and washed by centrifugation at 500g for 5 minutes at 4°C, followed by replacement of the supernatant with 20µl HBSS. A Countess 3 automated cell counter was used to calculate cell density and 7,000 live cells were loaded on to each channel of the Single Cell chip (10X Genomics). Single cells were encapsulated in droplets using the Chromium Controller (10X Genomics). Sequencing libraries were

prepared using the Chromium Single Cell 3' kit v3 as per the manufacturer's protocol. The LabChip GX Touch Nucleic Acid Analyser was used to quantify the concentration and quality of the libraries. Libraries were sequenced on a single Illumina Novaseq S3 flow cell with 300-400 million raw reads per sample.

Analysis of single cell RNA-sequencing data

Alignment, quality control and cleaning of scRNA-seq data

The 10X single cell RNA-seq data was demultiplexed, aligned and quantified using the CellRanger pipeline (10x Genomics Cell Ranger 3.1.0) and the Ensembl GRCz11.101 reference genome. Cells with fewer than 500 genes detected and cells which possessed greater than 12 percent mitochondrial reads were removed. Genes that were expressed within less than 2 cells were also removed. Ambient RNA was detected and removed using SoupX [90]. To detect doublets, three methods were used: doubletCells from scran, Scrublet [91] and DoubletDecon [92]. For the former two methods, a cut-off score was determined by inspecting a histogram to identify an outlying population with high doublet scores. Cells that were called doublets by at least two of these methods were discarded.

Normalisation, scaling, feature selection and cell cycle regression

SCTransform [93] was used to perform normalisation, scaling and selection of highly variable genes. This package was also used to regress out cell cycle signatures. Genes related to "S" and "G2M" phases of the cell cycle were identified using the Gene Ontology data base for Danio rerio. Genes associated with the following GO terms were assigned to the "S phase" gene list: "DNA replication", "DNA repair" and "mitotic DNA replication". Genes associated with the following GO terms were assigned to the "G2M phase" gene list: "chromosome

segregation", "mitotic nuclear division" and "mitotic cytokinesis". Genes which overlapped between the two lists were removed. The following genes were added manually to the "S phase" gene list: *ccnd1, ccnd2a, ccnd2", ccnd3, ccne1, ccne2, meis1b, ccne1, ccne2, ccna1, ccna2, cdc6, mcm2, mcm3, mcm4, mcm5, mcm6, mcm7, mcm10, orc1,* and *orc6.* The following genes were added manually to the "G2M phase" gene list: *ccna1, ccna2, foxm1, skp2, cdk1, ccnb1, ccnb2, ccnb3, mki67, top2a, oip5, nusap1, kif20a, kif23, racgap1, sgo1* and *anln*. Cell cycle scoring was performed in Seurat.

Dimensionality reduction and clustering

Principle components were calculated using scater and, where required, integrated between samples using Harmony [39]. Two-dimensional visualisation was performed using Uniform Manifold Approximation and Projection (UMAP). Graph based clustering was then performed by 1) construction of a network graph in scran, and 2) Louvain community detection with igraph. A range of k-nearest neighbour values were used to vary the granularity, and the final clustering was chosen on the basis of modularity and the expression of a priori markers.

Differential abundance analysis

Differential abundance of the various skin cell types between conditions was tested using EdgeR. The estimateDisp function was used to estimate negative binomial dispersion, the quasi-likelihood dispersion was estimated by glmQLFit and testing was performed by glmQLFTest.

Differential expression analyses

Pseudobulk differential expression analysis were performed on cells of equivalent type between the CAAX and HRAS samples using EdgeR. The clean counts per cell were summed across groups and normalised. The negative binomial dispersion of each group was calculated with estimateDisp, the quasi-likelihood dispersion was estimated using glQLFit and testing was carried out with glmQLFTest. Single cell differential expression analyses between clusters were performed using the findMarkers function from scran. Welch's t-tests were used to compare each cluster versus the sample. Wilcoxon Rank Sum Tests were performed between each pairwise combination of clusters to narrow down specific genes. Results from all differential expression analyses were filtered to include only genes that were expressed with >10% cells per cluster of interest, and FDR < 0.05. To identify the optimal markers of the PNC clusters, three tests were used with the following thresholds: pairwise Welch's t-tests (fold-change > 2), pairwise Wilcoxon Rank Sum tests (are under the curve > 0.8), and pairwise Binomial tests (fold-change > 2), and genes were filtered for expression with > 75% of cells within the cluster of interest.

Gene set enrichment analysis

The Gene Set Enrichment Analysis (GSEA) software (version 4.2.2) from The Broad Institute was implemented to test for enrichment of Biological Processes from the *Danio rerio* Gene Ontology database. Enrichment was considered significant with FDR < 0.1.

Over-representation analysis

Over-representation analysis was performed upon pseudobulk differential expression results using a hypergeometric test in fgsea. The gene sets for "immature Basal Epidermis" and "Mature Basal Epidermis" were derived from a scRNA-seq time course of zebrafish

embryonic development (Wagner et al. 2018). Nascent epidermal cells (10pf) were compared with developed epidermal cells (24hpf) using Welch's T-test and gene sets derived by filtering these results by FDR < 0.05, fold change > 1.25 and detected in > 10% of cells within the group of interest. The gene sets for "Upregulated by *tp63*" and "Downregulated by *tp63*" were taken directly from Santos-Pereira et al. 2019 [94], who performed transcriptomic comparison between tp63 knockout versus wildtype zebrafish larvae. The gene sets for "Basal Keratinocyte", "Superficial Keratinocyte" and "All Keratinocyte" were taken directly from Cokus et al. 2019, who performed a transcriptomic comparison of the basal keratinocytes and superficial keratinocytes of 72dpf zebrafish larvae in comparison to all keratinocytes and non-keratinocytes.

Inferring pseudotime trajectories

Trajectory analysis was performed using Monocle 3 [45]. The clean counts from the PNCs of the HRAS samples were re-normalised and batch corrected, followed by dimensionality reduction and clustering by the standard pre-processing guidelines for Monocle 3, prior to ordering and scoring by pseudotime. The cells within the 8hpi samples that most resembled their basal keratinocyte cells of origin were selected as the root.

Cross-species integration of scRNA-seq datasets

Human orthologues of zebrafish genes were acquired from the Alliance of Genome Resources and multi-mapping genes were excluded from downstream analysis. ScRNA-seq data from human cutaneous squamous cell carcinoma tumours and healthy skin was obtained from Ji et al. 2020 (GSE144240) and merged with the scRNA-seq data from keratinocytes and PNCs published herein. LIGER [45] was utilised to directly integrate the two

data sets as follows. Firstly, the merged datasets were re-normalised, scaled and highly variable genes selected according to LIGER default settings. Joint matrix factorisation was performed (k = 15) and the resulting factors were manually inspected. Factors dominated by cell cycle genes and ribosomal genes were excluded from downstream analysis. Finally, the datasets were integrated by quantile normalisation and jointly clustered using Louvain community detection.

FACS analysis of transgenic Arg2 reporter

Single cell suspensions from dissociated larvae in 5 mL FACS tubes were stained with 1:1000 DAPI (Thermofisher, #62248) to indicate cell viability and FACS was carried out at the QMRI Flow facility using a BD 5 Laser LSR Fortessa cell analyser. Arg2:EGFP positive cells were detected using the B525/50 laser. lysC:NLS-mScarlet positive neutrophils were detected using the YG610/20 laser. Live cells stained with DAPI were detected using the V450/50 laser. The panel of controls described in supplement material was used to apply compensation to the samples. The gating strategy used is shown in supplement material. All data was analysed in FlowJo v10.8.1 software (BD Life Sciences).

Confocal imaging & in vivo live imaging

All confocal fluorescent images were acquired with Leica confocal SP8, using HCX PL APO 40x water immersion objective lens. Appropriate lasers and collection gates were selected according to excitation and emission wavelength for each fluorophore. For in vivo live imaging data presented in figure 1, 2, 5, larvae were immobilized in 1% low-melting agarose in a glass bottom dish filled with 0.3 X DANEAU's solution. The whole-body neutrophil

imaging was carried out using a VAST system; in brief, anaesthetised larvae were transferred to individual wells of a 96-well plate in 300µl 0.3XDANEAU's solution. Larvae were then automatically loaded, positioned, and imaged one by one using the Vertebrate Automated Screening Technology (VAST) BioImager system (Union Biometrica) with incorporated Zeiss spinning disk confocal microscope (VAST-SDCM) (Early et al., 2018). The entire flank of each larva was imaged, excluding the head and distal end of the tail.

Image data analysis

Confocal SP8 image data analyses were carried out using IMARIS 9.0. Percentage of EdU or TUNEL positive cells within EGFP positive cells were manually counted. Quantification of EdU signal within GFP positive cells was performed manually by inspecting each optical section of image Z--stacks. For quantification of EdU signal in neighbouring cells, the remaining EdU positive nuclei, not within EGFP positive cells, were manually labelled using the Spots module. Then, GFP positive cells were isolated using the Surfaces module based on absolute GFP intensity. The function "The Spots Close To Surface XTension" allowed segregation of the spots subset within 10 µm distance to the nearest point of the Surface objects (GFP positive). Proliferating neighbouring cells are shown as a proportion of the number of spots in that subset to the number of GFP-HRas^{G12V} or GFP-CAAX positive cells. Quantification of TUNEL signal within GFP positive cells was performed manually by optical sectioning from TUNEL labelling images. Neutrophil and macrophage footprint analysis were carried out using Volocity 6.3 (Perkin Elmer) tracking fluorescent object function. Time-lapse videos were exported from Volocity or ImageJ and annotations were added using ImageJ.

Statistical analysis

Appropriate parametric or non-parametric tests to determine differences in mean or rank were carried out using Graphpad Prism 9.1.4 software (San Diego, USA). Degrees of freedom were calculated from the number of individual larvae measured. Graphs depict mean ± standard deviation (SD) unless otherwise stated. Null hypotheses were rejected when $p < 0.05$.

PanCancer RNA-seq analysis

Finalised RNA-seq and mutation data from the Pan-Cancer Atlas, generated by the Cancer Genome Atlas (TCGA), were obtained from the Genomic Data Commons portal (https://gdc.cancer.gov/)[82]. RAS mutation status was then inferred by non-silent mutation of KRAS, NRAS, or HRAS at residues G12, G13, and Q61, which are believed to account for 98% of all RAS mutations [95]. In order to assess expression of the HRAS-PNC-3 cluster genes within the context of mutation status, the collective expression of the top 30 differentially expressed genes within the signature was quantified as a single metric via gene set variation analysis (GSVA) [96]. Survival statistics were calculated and plotted for cancer-types with >10% RAS mutation frequency using the survival and survminer R packages, with patients stratified by high/low expression using thresholds calculated via the SurvivALL package [97].

Acknowledgement

The authors thank the technical support from the Confocal Advanced Light Microscopy facility in the Queen's Medical Research Institute, The High Content Screening Facility in the Institute for Regeneration and Repair and the BVS Aquatic Facility Units at the University of Edinburgh. The results shown in Figure 6 G are based upon data generated by the TCGA

Research Network: https://www.cancer.gov/tcga. The authors acknowledge fundings from Wellcome Trust Sir Henry Dale Fellowship to Y.F. (100104/Z/12/Z); Cancer Research UK Early Detection Award to Y.F. (C38363/A26931); A.M.E. was supported by a Medical Research Council PhD Studentship (MR/N013166/1); H. M. was supported by a postdoctoral fellowship from the Sigrid Jusélius Foundation. P.M.E. is funded by a Sir Henry Dale Fellowship, jointly funded by the Wellcome Trust and the Royal Society (Grant Number 105570/Z/14/A); C. G. H & R. C are funded by Worldwide Cancer Research (19-0238), Wellcome Trust ISSF 3 (UoE) and LifeArc-CSO; N.C.H is funded by a Wellcome Trust Senior Research Fellowship (219542/Z/19/Z).

Figure Legends

Figure 1) Oncogenic RAS drives enhanced cell proliferation in PNCs and neighbours within 24 hours of expression. A, schematic showing the protocol for inducing mosaic expression of HRAS^{G12V} within the basal epidermis of zebrafish larvae. **B,** wide-field fluorescent image of a 2dpf transgenic larva before 4-OH-tamoxifen induction, showing EGFP positive heart as selection marker. **C,** wide-field fluorescent image of a control larva expressing EGFP-CAAX in keratinocytes at 24 hours post induction (hpi). **D,** wide-field fluorescent image of a larva expressing EGFP-HRAS^{G12V} in keratinocytes at 24hpi. **E,** confocal image of a control larva with EGFP-CAAX positive keratinocytes, **E'** enlarged section from E. **F,** confocal image of a larva carrying EGFP-HRAS^{G12V} positive PNCs, **F'** enlarged section from F. **G,** still images from a time-lapse movie showing some EGFP high PNCs undergo apoptosis from 18hpi onwards

(Supplementary Movie 1). **H,** confocal images showing TUNEL (magenta) positive PNCs (Green), the white lines in H' indicate positions of cross-sections shown in H'', white arrowheads indicate TUNEL signal within PNCs; in 1 TUNEL signal is apical to PNCs. **I,** quantification of TUNEL positive PNCs showing increased apoptotic cell death at 24hpi (Mann Whitney test, p<0.0001, n=15). **J,** confocal images showing EdU staining (magenta) in control keratinocytes (CAAX) vs PNCs (HRAS), yellow arrowheads indicate EdU signal outside the PNCs (green). **K,** quantification of EdU positive PNCs showing increased PNC proliferation rate over time (two-way ANOVA Sidak's multiple comparison test, **** p<0.0001, n>=7). **L,** a schematic showing that neighbouring cells are defined as cells within 10μM of PNCs. **M,** quantification of EdU positive neighbouring cells showing increased proliferation over time (two-way ANOVA Sidak's multiple comparison test, * p=0.0209; *** p=0.0004; **** p<0.0001, n>=7).

Figure 2) Nascent RAS-driven PNCs elicit an immediate and sustained inflammatory response. A, a confocal still image from a time-lapse movie, showing neutrophils (magenta) are recruited to PNCs (green) as early as 5hpi, neutrophil tracks are shown (white lines). (Supplemental Movie 1) **B,** Quantification of the number of neutrophils observed within the epidermis of control versus PNC-bearing larvae at 5hpi (Mann-Whitney test, P<0.0001, n>=30). **C,** confocal still image from a time-lapse movie of control (EGFP-CAAX) epidermis showing almost no neutrophil (magenta) infiltration (Supplementary Movie 2). **C',** red areas indicate neutrophil footprints from the movie in C. **D,** confocal still image from a time-lapse movie showing neutrophils (magenta) infiltrated into PNC-bearing (EGFP-HRAS^{G12V}) epidermis (Supplementary Movie 2). **D',** red areas indicate neutrophil footprints from the

moive in D. **E,** quantification of pro-inflammatory cytokine expression by quantitative RT-PCR (unpaired t test, p<=0.0008, n=9). **F,** quantification of neutrophil infiltration into the epidermis of control (CAAX) versus PNC-bearing (HRAS) larvae from 12-36 hpi (two-way ANOVA, p<0.0001, n=10). **G,** a confocal still image from a time-lapse movie showing macrophages (green) in control larval epidermis with EGFP-CAAX positive keratinocytes (grey) (Supplementary Movie 3). **G'**, macrophage footprints (orange) from the movie in G, showing macrophage patrolling in larval epidermis. **H,** a confocal still image from a time-lapse movie showing macrophages (green) in PNC-bearing larval epidermis (mCherry-HRASG12V) (grey). (Supplementary Movie 3) **H'**, macrophage footprints (orange) from the movie in H, showing macrophage recruitment to PNCs. **I,** a confocal still image from a time-lapse movie showing macrophage (magenta) engulfing (white arrowhead) apoptotic PNCs (green). (Supplementary Movie 4). **J,** quantification of macrophage numbers in the epidermis of control (CAAX) versus PNC-bearing (HRAS) larvae from 12-36hpi (two-way ANOVA, p<0.0265, n>= 6).

Figure 3) scRNA-seq resolves transcriptomically distinct subsets of basal keratinocyte derived PNCs

A, UMAP visualisation of keratinocytes and PNCs derived from CAAX and HRAS larvae at 8 and 24 hpi. **B,** UMAP visualisation of keratinocytes and PNCs by cluster. **C,** The number of differentially upregulated genes versus all other clusters (pairwise Wilcoxon rank sum tests, genes filtered by detection in >10% of cells within at least one cluster per pair, FDR < 0.05). **D,** Heatmap depicting the scaled and centred expression of the top 30 enriched genes per cluster (Welch's T test between each cluster versus sample. Genes were filtered by

detection in >10% of cells within cluster, FDR < 0.05, fold-change >1, and ordered by fold change). **E,** Pseudotime trajectory analysis of PNC development predicted by Monocle 3, projected onto UMAP visualisation of PNCs derived from HRAS larvae only, coloured by cluster. **F,** Violin plots showing normalised expression of selected markers for PNC-3 (*lamc2*) and PNC-4 (*cldna*). **G,** Whole-mount HCR fluorescence in situ RNA detection showing heterogenous expression of PNC cluster markers *lamc2* (magenta) and *cldna* (yellow) within EGFP-HRAS^{G12V} PNCs (green) a 24hpi. Lower panel showing *lamc2* and *cldna* expression are largely mutually exclusive, Scale bar= 30µm.

Figure 4) Oncogenic RAS drives de-differentiation of basal keratinocytes and the re-expression of an embryonic epidermal programme

A, Heatmap depicting the scaled and centred expression of the top 100 downregulated genes in each PNC cluster, (PNC clusters were compared with all control basal keratinocytes by pseudobulk differential expression analysis. Genes were filtered by detection in >10% of cells within at least one group, FDR < 0.05, fold-change > |1.5|). **B,** Violin plots showing normalised expression of *tp63* in control (CAAX) basal keratinocytes, PNC clusters and superficial keratinocytes (Sup.). **C,** Over-representation analysis of gene-sets relating to epidermal development. Plot shows the significance of enrichment amongst genes downregulated (blue) and upregulated (red) in each PNC cluster at 24hpi. **D,** Gene Set Enrichment Analysis of Gene Ontology "Biological Processes" for each PNC cluster vs. control basal keratinocytes. Colours represent normalised enrichment score, radius represents q-value. **E,** Violin plots showing normalised expression of epigenetic stem cell

maintenance genes in control CAAX basal keratinocytes, PNC clusters and superficial keratinocytes.

Figure 5) PNC subsets correspond with subsets of cancer cells within SCC patient tumours, featuring mutually exclusive features of partial EMT versus suprabasal differentiation.

A, UMAP visualisation of basal keratinocytes and PNCs integrated with scRNA-seq data of basal cells from cutaneous squamous cell carcinomas patients and matched healthy skin [16]. Integration was performed using LIGER. Colours indicate clusters derived from the integrated dataset. **B,** UMAP visualisation of the cells from the Ji et al. dataset Colours indicate clustering performed in the original publication. **C,** UMAP visualisation of the zebrafish basal keratinocytes and PNCs. **D,** Quantification by cluster shows that the majority of "Tumour – Diff" cells belong to cluster 7, whilst the majority of "Tumour Specific" cells belong to cluster 11. **E,** Quantification by cluster shows that the majority of PNC-4 cells belong to cluster 7, whilst cluster 11 is enriched for PNC-3 cells. **F,** Over-representation analysis of gene-sets derived from the transcriptomic comparison of basal versus superficial keratinocytes in the zebrafish epidermis [44]. Plot shows the significance of enrichment amongst genes downregulated (blue) and upregulated (red) in each PNC cluster at 24hpi. **G,** Dot plot showing the scaled expression of EMT related genes, selected by significant upregulation in PNC-3. (Genes were filtered by detection in >10% of cells within PNC-3, FDR < 0.05, fold-change > 1.25). **H,** Relative expression of EMT related genes (*arpc5a*, *snai2*, *mmp9*, *itgb1b*, *itga5*, *itga3a*) in PNCs vs. control keratinocytes at 24hpi, measured by q-PCR.

I, confocal live imaging images showing PNCs (green) change shape over time. Yellow arrowhead highlights a cell with elongated shape and magenta arrowhead highlights a cell transitioning from round to elongated. **J,** quantification of cell shape distribution changes between 12hpi to 24hpi. **K** still confocal images from a time-lapse movie showing the membrane dynaimics of PNCs (green) at 24hpi, white arrowheads indicate protrusions from three individual cells, white asterisks indicate cells that maintain a round shape and lack membrane dynamics (Supplementary Movie 5). **L,** still confocal images from a time-lapse movie showing PNCs (green) become motile and start to migrate at approx. 24hpi. Each coloured asterisks indicates a cell that changed position in the time-lapse movie. (Supplemental Movie 6)

Figure 6) The PNC-3 cluster possesses cancer stem cell features and the PNC-3 gene signature is associated with poor prognosis in multiple cancer types

A, dot plot showing that the PNC-3 cluster up-regulates many mesenchymal marker genes and several epithelial marker genes (dot colour represents the level of expression, dot area represents the percentage of positive cells). **B,** dot plot showing that putative cancer stem cells markers and simple keratins are enriched in the PNC-3 cluster. **C,** Whole-mount HCR fluorescence in situ RNA detection showing the expression of simple keratin 18 (turquoise), a cancer stem cell marker, within a sub-population of PNC-3 (*lamc2*, magenta) cells, arrowhead indicates three clusters of *krt18* positive cells. **D,** UMAPs depicting the predicted cell cycle phase of each PNC and control keratinocyte calculated by Seurat cell cycle scoring algorithm. CAAX cells only (left) and HRAS PNCs only (right). **E,** Quantification of the percentage of cells predicted to belong to each cell cycle phase within each PNC cluster and

the CAAX control group. **F,** Heatmap showing the scaled normalised expression of genes related to EMT, S phase and G2M phase within the cells of the PNC-3 cluster only. Cells are grouped by predicted cell cycle phase. **G,** Kaplan-Meier curves show overall survival in patients across the primary RAS-driven cancer types. Patients are split according to expression of PNC-3 cluster genes, with those with high PNC-3 marker gene expression (red lines) exhibiting a significantly reduced overall survival than those with low expression (blue lines). P-values and hazard ratios were calculated using log-rank tests and Cox proportional hazard models, respectively.

Figure 7) RAS-driven PNCs elicit a systemic neutrophil response involving alterations to granulopoiesis within 24 hours

A, UMAP visualisation of unsupervised clustering of neutrophils from CAAX larvae (C1-5) and HRAS larvae (H1-4) at 8hpi, upper panel coloured by cluster; lower panels coloured by genotype CAAX (yellow) and HRAS (blue). **B,** UMAP visualisation of unsupervised clustering of neutrophils from CAAX larvae (C1-4) and HRAS larvae (H1-4) at 24hpi, upper panel coloured by cluster, lower panels coloured by genotype CAAX (yellow) and HRAS (blue). **C,** Dot plot representing the expression of genes associated with Granulocytic Myeloid Progenitors, immature neutrophils and mature neutrophils. (Dot area represents the percentage of cells in which each was detected, colour represents the scaled average expression within positive cells). **D,** The top 50 upregulated genes expressed in each control neutrophil cluster (C1-4) versus the remaining neutrophils at 24hpi. Hierarchical clustering of cell groups shows each neutrophil cluster from PNC-bearing larvae (H1-4) paired with its matched control cluster. (Non-unique genes are included in the cluster in which they first appear in numerical order. Gene expression values are scaled and centered around zero.

Differential expression was determined by Welch's T-test between the cell of a given cluster and the cells from all remaining neutrophil clusters. Genes were filtered by detection in at least 10% of the cells within the given cluster and FDR < 0.05, then ranked by fold-change). **E,** The percentage of neutrophils belonging to each maturity group within control © and PNC-bearing larvae (H) at 8 and 24hpi. **F,** Fluorescent images of neutrophils, Tg(*lyz:nls-scarlet*) (grey) in a control larva (CAAX) and a PNC-bearing (HRAS) larva. Boxed areas indicate Central Haematopoietic Tissue (CHT) region. Scale bar = 100µm. **G,** Quantification of the mean area of fluorescence within the whole image, the CHT region, and the percentage of the total area outwith the CHT. **H,** Quantification of the mean fluorescence intensity within the whole image, the CHT region, and the area outwith the CHT. N = 10 (CAAX), 13 (HRAS). (Welch's t-tests, ****: P < 0.0001).

Figure 8) Neutrophils from PNC-bearing larvae express immunosuppressive marker arginase 2 and promote PNC proliferation

A, Heatmap depicting log2 fold change of pro-tumour TAN marker genes, *arg2* and *ptges3b*, and pro-inflammatory genes, *il1b* and *cybb* in the neutrophil clusters from PNC-bearing larvae versus their equivalent clusters from control larvae. **B,** dot plot showing the expression of *tgfb1a*, *csf3b* (g-csf) and *il1b* genes within PNCs and control keratinocytes (dot area represents the percentage of cells in which each was detected, colour represents the scaled average expression within positive cells). **C & D,** confocal live imaging of transgenic *arg2* reporter in expressed within neutrophils of PNC-bearing larvae versus sibling controls. **C i,** schematic showing the regions of the epidermis and the CHT that were imaged. **C ii,** neutrophils in CHT of a control larva; **C iii,** neutrophils in CHT of a PNC-bearing larva; **C iv,** single channel showing no *arg2* reporter expression in the CHT of the control larva; **C v**,

single channel showing *arg2* reporter expression in the CHT of the PNC-bearing larva, white arrowheads showing *arg2* reporter expression in neutrophils. **D i,** neutrophil (magenta) and *arg2* reporter (turquoise) in a sibling control larva; **D ii,** single channel showing no arg2 reporter expression in neutrophils in the epidermis of the control larva; **D iii,** neutrophils (magenta) expressing *arg2* reporter (turquoise) in the epidermis of the PNC-bearing larva. **D iv,** two channel image showing neutrophils (magenta) expressing *arg2* reporter (turquoise) in the PNC-bearing larva. **D v**, single channel showing *arg2* reporter. Scale bar = 30µm. **E**, quantification of *arg2* positive neutrophils in the CHT (Welch's t test n>=13, p<0.0001). **F,** quantification of *arg2* positive neutrophils in images taken from the epidermis (Welch's t test, n>= 12 p<0.0001). **G,** quantification of *arg2* expression in FACS sorted neutrophils from PNC-bearing larvae (HRAS) versus sibling controls (Unpaired *t* test, n=3, p<0.0001). **H,** the percentage of EdU positive PNCs in larvae injected with *csf3r* morpholino versus control morpholino (Mann-Whitney test, n>=26, p<0.0001). **I,** violin plots showing the normalised expression of *cxcl8a* and *cxcl8b.1* within keratinocytes and PNCs. **J,** violin plots showing the expression of *cxcr1* within neutrophils at 24hpi. **K,** quantification of numbers of neutrophils in direct contact with PNCs from confocal images taken from 24hpi PNC bearing larvae, in larvae treated with reparixin (cxcr1 inhibitor) and SB225002 (cxcr2 inhibitor) versus DMSO treated larvae. One way ANOVA test with Dunnett's multiple comparisons test, n>=14, p=0.0254. **L,** quantification of EdU positive PNCs in larvae treated with reparixin (cxcr1 inhibitor) and SB225002 (cxcr2 inhibitor) versus DMSO treated larvae (One-way ANOVA test with Dunnett's multiple comparisons test, n>=14, p=0.0002).

Supplementary

Supplementary Figure 1) Identification of cell types in scRNA-seq data by cluster-enriched marker genes.

A, Schematic of experimental workflow for scRNA-seq sample preparation. mCherry-labelled PNCs and EGFP-labelled myeloid cells were obtained from "HRAS" larvae = *Tg(mpeg1:EGFP; krtt1c19e:KalTA4-ER^{T2};UAS:mcherry-HRAS^{G12V}).* mCherry-labelled wildtype keratinocytes and EGFP-labelled myeloid cells were obtained from "CAAX" larvae = *Tg(mpeg1:EGFP; krtt1c19e:KalTA4-ER^{T2};UAS:mcherry-CAAX).* Larvae were induced at 3dpf with 4-hydroxytamoxifen and dissociated by collagenase digest at 8 and 24hpi. 150 larvae were pooled per sample and both mCherry positive and EGFP positive cells were sorted into the same tube for processing on the 10X Chromium platform. The table indicates the number of high-quality cells per sample following sequencing and quality control.

B, UMAP visualisation of cells from all six samples following unsupervised clustering.

C, UMAPs depicting the normalised expression of key cell type markers for keratinocytes (*krtt1c19e*), basal keratinocytes (*tp63*), superficial keratinocytes (*cldne*), myeloid cells (*EGFP*), macrophages (*mpeg1.1*) and neutrophils (*lyz*). **D,** Dotplot depicting the scaled expression of an expanded panel of cell type specific markers. **E,** UMAP visualisation of skin cells (clusters 1-8) from CAAX control larvae (yellow) and HRAS larvae (blue) at 24hpi.

F, The percentage of total skin cells assigned to each cluster, tested for differential abundance between HRAS-24hpi and CAAX-24hpi samples. **G,** The number of differentially expressed genes for each cell type within the HRAS-24hpi samples versus the corresponding cell type within CAAX-24hpi samples (FDR < 0.05, fold-change > |1.5|).

UMAP: Uniform Manifold Approximation Projection, FDR: False Discovery Rate.

Supplementary Figure 2) At 24hpi, the macrophage response to PNC initiation is minimal and has no effect on PNC proliferation.

A, UMAP visualization of macrophages, dendritic cells and microglia from 24hpi scRNA-seq samples, coloured by cluster. **B,** UMAP visualization coloured by condition, i.e., CAAX control larvae and HRAS PNC-bearing larvae. **C,** Quantification of the percentage of cells per cluster. **D,** Dot plot showing the expression of macrophage, microglia, dendritic cells and neutrophil markers. **E,** The number of differentially expressed genes identified between CAAX and HRAS samples for each cluster depicted. (Welch's T-tests. Genes were filtered by expression in at least 10% of cells within at least one of the groups compared, FDR < 0.05 and fold change > |1.25|). **F,** The log2 fold change of genes related to the pro-inflammatory or alternative activation of macrophages. **G,** Quantification of PNC number (i) and the percentage of EdU positive PNCs (ii) from PNC-bearing larvae lacking macrophages due to *irf8* Morpholino injection versus control Morpholino. n=14 (irf8 Mo), n=11 (control Mo), Welch's t-tests, ns = P >0.05. **H,** Quantification of PNC number (i) and the percentage of EdU positive PNCs (ii) from PNC-bearing larvae depleted of macrophages by injection with Liposome Clodronate (L-Clod). n=16, Welch's t-tests, ns = P >0.05.

References

1. Crosby, D., Bhatia, S., Brindle, K.M., Coussens, L.M., Dive, C., Emberton, M., Esener,

S., Fitzgerald, R.C., Gambhir, S.S., Kuhn, P., et al. (2022). Early detection of cancer. Science (80-.). *375*, aay9040.

2. Rane, J.K., Frankell, A.M., Weeden, C.E., and Swanton, C. (2023). Clonal Evolution in Healthy and Premalignant Tissues: Implications for Early Cancer Interception Strategies. Cancer Prev. Res. *16*, 369–378. 10.1158/1940-6207.CAPR-22-0469/718823/AM/CLONAL-EVOLUTION-IN-HEALTHY-AND-PREMALIGNANT.

3. McGranahan, N., and Swanton, C. (2017). Clonal Heterogeneity and Tumor Evolution: Past, Present, and the Future. Cell *168*, 613–628. 10.1016/J.CELL.2017.01.018.

4. Wijewardhane, N., Dressler, L., and Ciccarelli, F.D. (2021). Normal Somatic Mutations in Cancer Transformation. Cancer Cell *39*, 125–129. 10.1016/j.ccell.2020.11.002.

5. Bozic, I., and Wu, C.J. (2020). Delineating the evolutionary dynamics of cancer from theory to reality. Nat. Cancer 2020 16 *1*, 580–588. 10.1038/s43018-020-0079-6.

6. Elliot, A., Myllymäki, H., and Feng, Y. (2020). Inflammatory Responses during Tumour Initiation: From Zebrafish Transgenic Models of Cancer to Evidence from Mouse and Man. Cells 2020, Vol. 9, Page 1018 *9*, 1018. 10.3390/CELLS9041018.

7. Balmain, A. (2022). Peto's paradox revisited: black box vs mechanistic approaches to understanding the roles of mutations and promoting factors in cancer. Eur. J. Epidemiol. *1*, 1–8. 10.1007/S10654-022-00933-X/FIGURES/1.

8. Yokoyama, A., Kakiuchi, N., Yoshizato, T., Nannya, Y., Suzuki, H., Takeuchi, Y., Shiozawa, Y., Sato, Y., Aoki, K., Kim, S.K., et al. (2019). Age-related remodelling of oesophageal epithelia by mutated cancer drivers. Nature *565*, 312–317.

10.1038/S41586-018-0811-X.

9. Li, R., Di, L., Li, J., Fan, W., Liu, Y., Guo, W., Liu, W., Liu, L., Li, Q., Chen, L., et al. (2021). A body map of somatic mutagenesis in morphologically normal human tissues. Nat. 2021 5977876 *597*, 398–403. 10.1038/s41586-021-03836-1.

10. Martincorena, I., Roshan, A., Gerstung, M., Ellis, P., Van Loo, P., McLaren, S., Wedge, D.C., Fullam, A., Alexandrov, L.B., Tubio, J.M., et al. (2015). High burden and pervasive positive selection of somatic mutations in normal human skin. Science (80-.). *348*, 880–885. 10.1126/science.aaa6806.

11. Lee-Six, H., Olafsson, S., Ellis, P., Osborne, R.J., Sanders, M.A., Moore, L., Georgakopoulos, N., Torrente, F., Noorani, A., Goddard, M., et al. (2019). The landscape of somatic mutation in normal colorectal epithelial cells. *574*, 532–537. 10.1038/s41586-019-1672-7.

12. Risques, R.A., and Kennedy, S.R. (2018). Aging and the rise of somatic cancer-associated mutations in normal tissues. PLOS Genet. *14*, e1007108. 10.1371/JOURNAL.PGEN.1007108.

13. Martincorena, I., Fowler, J.C., Wabik, A., Lawson, A.R.J., Abascal, F., Hall, M.W.J., Cagan, A., Murai, K., Mahbubani, K., Stratton, M.R., et al. (2018). Somatic mutant clones colonize the human esophagus with age. Science (80-.). *362*, 911–917. 10.1126/SCIENCE.AAU3879/SUPPL_FILE/AAU3879_TABLES4.XLSX.

14. Fowler, J.C., and Jones, P.H. (2022). Somatic Mutation: What Shapes the Mutational Landscape of Normal Epithelia? Cancer Discov. *12*, 1642–1655. 10.1158/2159-

8290.CD-22-0145/694187/AM/SOMATIC-MUTATION-WHAT-SHAPES-THE-MUTATIONAL.

15. Kakiuchi, N., and Ogawa, S. (2021). Clonal expansion in non-cancer tissues. Nat. Rev. Cancer 2021 214 *21*, 239–256. 10.1038/s41568-021-00335-3.

16. Ji, A.L., Rubin, A.J., Thrane, K., Jiang, S., Reynolds, D.L., Meyers, R.M., Guo, M.G., George, B.M., Mollbrink, A., Bergenstråhle, J., et al. (2020). Multimodal Analysis of Composition and Spatial Architecture in Human Squamous Cell Carcinoma. Cell *182*, 497-514.e22. 10.1016/J.CELL.2020.05.039.

17. Cagan, R.L., Zon, L.I., and White, R.M. (2019). Modeling Cancer with Flies and Fish. Dev. Cell *49*, 317–324. 10.1016/J.DEVCEL.2019.04.013.

18. Li, S., Balmain, A., and Counter, C.M. (2018). A model for RAS mutation patterns in cancers: finding the sweet spot. Nat. Rev. Cancer 2018 1812 *18*, 767–777. 10.1038/s41568-018-0076-6.

19. Lawson, A.R.J., Abascal, F., Coorens, T.H.H., Hooks, Y., O'Neill, L., Latimer, C., Raine, K., Sanders, M.A., Warren, A.Y., Mahbubani, K.T.A., et al. (2020). Extensive heterogeneity in somatic mutation and selection in the human bladder. Science (80-.). *370*. 10.1126/SCIENCE.ABA8347.

20. Vishwakarma, M., and Piddini, E. (2020). Outcompeting cancer. Nat. Rev. Cancer 2020 203 *20*, 187–198. 10.1038/s41568-019-0231-8.

21. Tanimura, N., and Fujita, Y. (2020). Epithelial defense against cancer (EDAC). Semin. Cancer Biol. *63*, 44–48. 10.1016/J.SEMCANCER.2019.05.011.

22. Hill, W., Zaragkoulias, A., Salvador-Barbero, B., Parfitt, G.J., Alatsatianos, M., Padilha, A., Porazinski, S., Woolley, T.E., Morton, J.P., Sansom, O.J., et al. (2021). EPHA2-dependent outcompetition of KRASG12D mutant cells by wild-type neighbors in the adult pancreas. Curr. Biol. *31*, 2550-2560.e5. 10.1016/J.CUB.2021.03.094.

23. Gopinathan, A., Morton, J.P., Jodrell, D.I., and Sansom, O.J. (2015). GEMMs as preclinical models for testing pancreatic cancer therapies. Dis. Model. Mech. *8*, 1185–1200. 10.1242/DMM.021055.

24. Freisinger, C.M., and Huttenlocher, A. (2014). Live Imaging and Gene Expression Analysis in Zebrafish Identifies a Link between Neutrophils and Epithelial to Mesenchymal Transition. PLoS One *9*, e112183. 10.1371/JOURNAL.PONE.0112183.

25. Feng, Y., Santoriello, C., Mione, M., Hurlstone, A., and Martin, P. (2010). Live imaging of innate immune cell sensing of transformed cells in zebrafish larvae: Parallels between tumor initiation and wound inflammation. PLoS Biol. *8*. 10.1371/journal.pbio.1000562.

26. Feng, Y., Renshaw, S., and Martin, P. (2012). Live imaging of tumor initiation in zebrafish larvae reveals a trophic role for leukocyte-derived PGE<inf>2</inf>. Curr. Biol. *22*. 10.1016/j.cub.2012.05.010.

27. Fadul, J., Zulueta-Coarasa, T., Slattum, G.M., Redd, N.M., Jin, M.F., Redd, M.J., Daetwyler, S., Hedeen, D., Huisken, J., and Rosenblatt, J. (2021). KRas-transformed epithelia cells invade and partially dedifferentiate by basal cell extrusion. Nat. Commun. 2021 121 *12*, 1–9. 10.1038/s41467-021-27513-z.

28. Chang, W.J., and Hwang, P.P. (2011). Development of zebrafish epidermis. Birth Defects Res. Part C Embryo Today Rev. *93*, 205–214. 10.1002/BDRC.20215.

29. Lee, R.T.H., Asharani, P. V., and Carney, T.J. (2014). Basal Keratinocytes Contribute to All Strata of the Adult Zebrafish Epidermis. PLoS One *9*, e84858. 10.1371/journal.pone.0084858.

30. Winge, M.C.G., Kellman, L.N., Guo, K., Tang, J.Y., Swetter, S.M., Aasi, S.Z., Sarin, K.Y., Chang, A.L.S., and Khavari, P.A. (2023). Advances in cutaneous squamous cell carcinoma. Nat. Rev. Cancer 2023 237 *23*, 430–449. 10.1038/s41568-023-00583-5.

31. Balmain, A., and Pragnell, I.B. (1983). Mouse skin carcinomas induced in vivo by chemical carcinogens have a transforming Harvey-ras oncogene. Nat. 1983 3035912 *303*, 72–74. 10.1038/303072a0.

32. Oshimori, N., Oristian, D., and Fuchs, E. (2015). TGF-β Promotes Heterogeneity and Drug Resistance in Squamous Cell Carcinoma. Cell *160*, 963–976. 10.1016/J.CELL.2015.01.043.

33. Santoriello, C., Gennaro, E., Anelli, V., Distel, M., Kelly, A., Köster, R.W., Hurlstone, A., and Mione, M. (2010). Kita Driven Expression of Oncogenic HRAS Leads to Early Onset and Highly Penetrant Melanoma in Zebrafish. PLoS One *5*, e15170. 10.1371/JOURNAL.PONE.0015170.

34. Hanahan, D., and Weinberg, R.A. (2011). Hallmarks of cancer: The next generation. Cell *144*, 646–674. 10.1016/j.cell.2011.02.013.

35. Downward, J. (1998). Ras signalling and apoptosis. Curr. Opin. Genet. Dev. *8*, 49–54.

10.1016/S0959-437X(98)80061-0.

36. Morana, O., Wood, W., and Gregory, C.D. (2022). The Apoptosis Paradox in Cancer. Int. J. Mol. Sci. 2022, Vol. 23, Page 1328 *23*, 1328. 10.3390/IJMS23031328.

37. Powell, D., Lou, M., Barros Becker, F., and Huttenlocher, A. (2018). Cxcr1 mediates recruitment of neutrophils and supports proliferation of tumor-initiating astrocytes in vivo. Sci. Reports 2018 81 *8*, 1–12. 10.1038/s41598-018-31675-0.

38. Chia, K., Mazzolini, J., Mione, M., and Sieger, D. (2018). Tumor initiating cells induce cxcr4- mediated infiltration of pro-tumoral macrophages into the brain. Elife *7*. 10.7554/ELIFE.31918.

39. Korsunsky, I., Millard, N., Fan, J., Slowikowski, K., Zhang, F., Wei, K., Baglaenko, Y., Brenner, M., Loh, P. ru, and Raychaudhuri, S. (2019). Fast, sensitive and accurate integration of single-cell data with Harmony. Nat. Methods 2019 1612 *16*, 1289–1296. 10.1038/s41592-019-0619-0.

40. Zhao, X., Jiang, M., and Wang, Z. (2019). TPM4 promotes cell migration by modulating F-actin formation in lung cancer . Onco. Targets. Ther. *12*, 4055–4063. 10.2147/OTT.S198542.

41. Liu, J., Zhang, Y., Li, Q., and Wang, Y. (2020). Transgelins: Cytoskeletal Associated Proteins Implicated in the Metastasis of Colorectal Cancer. Front. Cell Dev. Biol. *8*, 573859. 10.3389/FCELL.2020.573859/BIBTEX.

42. Staquicini, D.I., Rangel, R., Guzman-Rojas, L., Staquicini, F.I., Dobroff, A.S., Tarleton, C.A., Ozbun, M.A., Kolonin, M.G., Gelovani, J.G., Marchiò, S., et al. (2017).

Intracellular targeting of annexin A2 inhibits tumor cell adhesion, migration, and in vivo grafting. Sci. Reports 2017 71 *7*, 1–11. 10.1038/s41598-017-03470-w.

43. Hou, Y., Lee, H.J., Chen, Y., Ge, J., Osman, F.O.I., McAdow, A.R., Mokalled, M.H., Johnson, S.L., Zhao, G., and Wang, T. (2020). Cellular diversity of the regenerating caudal fin. Sci. Adv. *6*. 10.1126/SCIADV.ABA2084/SUPPL_FILE/ABA2084_TABLES_S1_TO_S7.XLSX.

44. Cokus, S.J., De La Torre, M., Medina, E.F., Rasmussen, J.P., Ramirez-Gutierrez, J., Sagasti, A., and Wang, F. (2019). Tissue-Specific Transcriptomes Reveal Gene Expression Trajectories in Two Maturing Skin Epithelial Layers in Zebrafish Embryos. G3 Genes|Genomes|Genetics *9*, 3439–3452. 10.1534/G3.119.400402.

45. Cao, J., Spielmann, M., Qiu, X., Huang, X., Ibrahim, D.M., Hill, A.J., Zhang, F., Mundlos, S., Christiansen, L., Steemers, F.J., et al. (2019). The single-cell transcriptional landscape of mammalian organogenesis. Nat. 2019 5667745 *566*, 496–502. 10.1038/s41586-019-0969-x.

46. Hanahan, D. (2022). Hallmarks of Cancer: New Dimensions. Cancer Discov. *12*, 31–46. 10.1158/2159-8290.CD-21-1059.

47. Bressan, R.B., and Pollard, S.M. (2020). Transcriptional and epigenetic regulatory mechanisms in glioblastoma stem cells. Stem Cell Epigenetics, 231–255. 10.1016/B978-0-12-814085-7.00010-6.

48. Pal, B., Chen, Y., Vaillant, F., Jamieson, P., Gordon, L., Rios, A.C., Wilcox, S., Fu, N., Liu, K.H., Jackling, F.C., et al. (2017). Construction of developmental lineage relationships

in the mouse mammary gland by single-cell RNA profiling. Nat. Commun. 2017 81 *8*, 1–14. 10.1038/s41467-017-01560-x.

49. Marjanovic, N.D., Hofree, M., Chan, J.E., Canner, D., Wu, K., Trakala, M., Hartmann, G.G., Smith, O.C., Kim, J.Y., Evans, K.V., et al. (2020). Emergence of a High-Plasticity Cell State during Lung Cancer Evolution. Cancer Cell *38*, 229-246.e13. 10.1016/J.CCELL.2020.06.012.

50. Saghafinia, S., Homicsko, K., Di Domenico, A., Wullschleger, S., Perren, A., Marinoni, I., Ciriello, G., Michael, I.P., and Hanahan, D. (2021). Cancer cells retrace a stepwise differentiation program during malignant progression. Cancer Discov. *11*, 2638–2657. 10.1158/2159-8290.CD-20-1637/674165/AM/CANCER-CELLS-RETRACE-A-STEPWISE-DIFFERENTIATION.

51. Perdigoto, C.N., Valdes, V.J., Bardot, E.S., and Ezhkova, E. (2014). Epigenetic Regulation of Epidermal Differentiation. Cold Spring Harb. Perspect. Med. *4*, a015263. 10.1101/CSHPERSPECT.A015263.

52. Bao, X., Tang, J., Lopez-Pajares, V., Tao, S., Qu, K., Crabtree, G.R., and Khavari, P.A. (2013). ACTL6a Enforces the Epidermal Progenitor State by Suppressing SWI/SNF-Dependent Induction of KLF4. Cell Stem Cell *12*, 193–203. 10.1016/J.STEM.2012.12.014.

53. Mulder, K.W., Wang, X., Escriu, C., Ito, Y., Schwarz, R.F., Gillis, J., Sirokmány, G., Donati, G., Uribe-Lewis, S., Pavlidis, P., et al. (2012). Diverse epigenetic strategies interact to control epidermal differentiation. Nat. Cell Biol. 2012 147 *14*, 753–763. 10.1038/ncb2520.

54. Liu, J., Gao, C., Sodicoff, J., Kozareva, V., Macosko, E.Z., and Welch, J.D. (2020). Jointly defining cell types from multiple single-cell datasets using LIGER. Nat. Protoc. *15*. 10.1038/s41596-020-0391-8.

55. Liu, S., Liang, J., Liu, Z., Zhang, C., Wang, Y., Watson, A.H., Zhou, C., Zhang, F., Wu, K., Zhang, F., et al. (2021). The Role of CD276 in Cancers. Front. Oncol. *11*, 654684. 10.3389/FONC.2021.654684/BIBTEX.

56. Vences-Catalán, F., Rajapaksa, R., Kuo, C.C., Miller, C.L., Lee, A., Ramani, V.C., Jeffrey, S.S., Levy, R., and Levy, S. (2021). Targeting the tetraspanin CD81 reduces cancer invasion and metastasis. Proc. Natl. Acad. Sci. U. S. A. *118*, e2018961118. 10.1073/PNAS.2018961118/SUPPL_FILE/PNAS.2018961118.SAPP.PDF.

57. Chu, W., Song, X., Yang, X., Ma, L., Zhu, J., He, M., Wang, Z., and Wu, Y. (2014). Neuropilin-1 Promotes Epithelial-to-Mesenchymal Transition by Stimulating Nuclear Factor-Kappa B and Is Associated with Poor Prognosis in Human Oral Squamous Cell Carcinoma. PLoS One *9*, e101931. 10.1371/JOURNAL.PONE.0101931.

58. Ray, T., Ryusaki, T., and Ray, P.S. (2021). Therapeutically Targeting Cancers That Overexpress FOXC1: A Transcriptional Driver of Cell Plasticity, Partial EMT, and Cancer Metastasis. Front. Oncol. *11*, 721959. 10.3389/FONC.2021.721959/BIBTEX.

59. Ding, X., Wang, X., Gong, Y., Ruan, H., Sun, Y., and Yu, Y. (2017). KLF7 overexpression in human oral squamous cell carcinoma promotes migration and epithelial-mesenchymal transition. Oncol. Lett. *13*, 2281–2289. 10.3892/OL.2017.5734/HTML.

60. Oliemuller, E., Newman, R., Tsang, S.M., Foo, S., Muirhead, G., Noor, F., Haider, S.,

Aurrekoetxea-Rodríguez, I., Vivanco, M.D.M., and Howard, B.A. (2020). Sox11 promotes epithelial/mesenchymal hybrid state and alters tropism of invasive breast cancer cells. Elife *9*, 1–29. 10.7554/ELIFE.58374.

61. Zeisberg, M., and Neilson, E.G. (2009). Biomarkers for epithelial-mesenchymal transitions. J. Clin. Invest. *119*, 1429–1437. 10.1172/JCI36183.

62. Cook, D.P., and Vanderhyden, B.C. (2020). Context specificity of the EMT transcriptional response. Nat. Commun. 2020 111 *11*, 1–9. 10.1038/s41467-020-16066-2.

63. Subbalakshmi, A.R., Sahoo, S., Biswas, K., and Jolly, M.K. (2022). A Computational Systems Biology Approach Identifies SLUG as a Mediator of Partial Epithelial-Mesenchymal Transition (EMT). Cells Tissues Organs *211*, 689–702. 10.1159/000512520.

64. Sterneck, E., Poria, D.K., and Balamurugan, K. (2020). Slug and E-Cadherin: Stealth Accomplices? Front. Mol. Biosci. *7*, 554454. 10.3389/FMOLB.2020.00138/BIBTEX.

65. Shibue, T., and Weinberg, R.A. (2017). EMT, CSCs, and drug resistance: the mechanistic link and clinical implications. Nat. Rev. Clin. Oncol. 2017 1410 *14*, 611–629. 10.1038/nrclinonc.2017.44.

66. Zhou, H.M., Zhang, J.G., Zhang, X., and Li, Q. (2021). Targeting cancer stem cells for reversing therapy resistance: mechanism, signaling, and prospective agents. Signal Transduct. Target. Ther. 2021 61 *6*, 1–17. 10.1038/s41392-020-00430-1.

67. Yuan, S., Stewart, K.S., Yang, Y., Abdusselamoglu, M.D., Parigi, S.M., Feinberg, T.Y.,

Tumaneng, K., Yang, H., Levorse, J.M., Polak, L., et al. (2022). Ras drives malignancy through stem cell crosstalk with the microenvironment. Nat. 2022 6127940 *612*, 555–563. 10.1038/s41586-022-05475-6.

68. Ellett, F., Pase, L., Hayman, J.W., Andrianopoulos, A., and Lieschke, G.J. (2011). mpeg1 promoter transgenes direct macrophage-lineage expression in zebrafish. Blood *117*, e49–e56. 10.1182/BLOOD-2010-10-314120.

69. Evrard, M., Kwok, I.W.H., Chong, S.Z., Teng, K.W.W., Becht, E., Chen, J., Sieow, J.L., Penny, H.L., Ching, G.C., Devi, S., et al. (2018). Developmental Analysis of Bone Marrow Neutrophils Reveals Populations Specialized in Expansion, Trafficking, and Effector Functions. Immunity *48*, 364-379.e8. 10.1016/J.IMMUNI.2018.02.002.

70. Ng, L.G., Ostuni, R., and Hidalgo, A. (2019). Heterogeneity of neutrophils. Nat. Rev. Immunol. 2019 194 *19*, 255–265. 10.1038/s41577-019-0141-8.

71. Kwok, I., Becht, E., Xia, Y., Ng, M., Teh, Y.C., Tan, L., Evrard, M., Li, J.L.Y., Tran, H.T.N., Tan, Y., et al. (2020). Combinatorial Single-Cell Analyses of Granulocyte-Monocyte Progenitor Heterogeneity Reveals an Early Uni-potent Neutrophil Progenitor. Immunity *53*, 303-318.e5. 10.1016/J.IMMUNI.2020.06.005.

72. Jin, H., Huang, Z., Chi, Y., Wu, M., Zhou, R., Zhao, L., Xu, J., Zhen, F., Lan, Y., Li, L., et al. (2016). c-Myb acts in parallel and cooperatively with Cebp1 to regulate neutrophil maturation in zebrafish. Blood *128*, 415–426. 10.1182/BLOOD-2015-12-686147.

73. Walters, K.B., Green, J.M., Surfus, J.C., Yoo, S.K., and Huttenlocher, A. (2010). Live imaging of neutrophil motility in a zebrafish model of WHIM syndrome. Blood *116*,

2803–2811. 10.1182/BLOOD-2010-03-276972.

74. Soza-Ried, C., Hess, I., Netuschil, N., Schorpp, M., and Boehm, T. (2010). Essential role of c-myb in definitive hematopoiesis is evolutionarily conserved. Proc. Natl. Acad. Sci. U. S. A. *107*, 17304–17308. 10.1073/PNAS.1004640107/SUPPL_FILE/SM10.GIF.

75. Manz, M.G., and Boettcher, S. (2014). Emergency granulopoiesis. Nat. Rev. Immunol. 2014 145 *14*, 302–314. 10.1038/nri3660.

76. Fridlender, Z.G., Sun, J., Kim, S., Kapoor, V., Cheng, G., Ling, L., Worthen, G.S., and Albelda, S.M. (2009). Polarization of Tumor-Associated Neutrophil Phenotype by TGF-β: "N1" versus "N2" TAN. Cancer Cell *16*, 183–194. 10.1016/J.CCR.2009.06.017.

77. Mizuno, R., Kawada, K., and Sakai, Y. (2019). Prostaglandin E2/EP Signaling in the Tumor Microenvironment of Colorectal Cancer. Int. J. Mol. Sci. 2019, Vol. 20, Page 6254 *20*, 6254. 10.3390/IJMS20246254.

78. Gabrilovich, D.I., Ostrand-Rosenberg, S., and Bronte, V. (2012). Coordinated regulation of myeloid cells by tumours. Nat. Rev. Immunol. 2012 124 *12*, 253–268. 10.1038/nri3175.

79. Shaul, M.E., and Fridlender, Z.G. (2018). Cancer-related circulating and tumor-associated neutrophils – subtypes, sources and function. FEBS J. *285*, 4316–4342. 10.1111/FEBS.14524.

80. Hammond, F.R., Lewis, A., Speirs, Z.C., Anderson, H.E., Sipka, T., Williams, L.G., Nguyen-Chi, M., Meijer, A.H., Wiegertjes, G.F., and Elks, P.M. (2023). An arginase 2 promoter transgenic line illuminates immune cell polarisation in zebrafish. Dis.

Model. Mech. *16*. 10.1242/DMM.049966.

81. van den Berg, M.C.W., MacCarthy-Morrogh, L., Carter, D., Morris, J., Ribeiro Bravo, I., Feng, Y., and Martin, P. (2019). Proteolytic and Opportunistic Breaching of the Basement Membrane Zone by Immune Cells during Tumor Initiation. Cell Rep. *27*. 10.1016/j.celrep.2019.05.029.

82. The Cancer Genome Atlas Program (TCGA) - NCI https://www.cancer.gov/ccg/research/genome-sequencing/tcga.

83. Lapouge, G., Beck, B., Nassar, D., Dubois, C., Dekoninck, S., and Blanpain, C. (2012). Skin squamous cell carcinoma propagating cells increase with tumour progression and invasiveness. EMBO J. *31*, 4563–4575. 10.1038/EMBOJ.2012.312.

84. Jamieson, T., Clarke, M., Steele, C.W., Samuel, M.S., Neumann, J., Jung, A., Huels, D., Olson, M.F., Das, S., Nibbs, R.J.B., et al. (2012). Inhibition of CXCR2 profoundly suppresses inflammation-driven and spontaneous tumorigenesis. J. Clin. Invest. *122*, 3127–3144. 10.1172/JCI61067.

85. Campbell, J.S., Davidson, A.J., Todd, H., Rodrigues, F.S.L.M., Elliot, A.M., Early, J.J., Lyons, D.A., Feng, Y., and Wood, W. (2021). PTPN21/Pez Is a Novel and Evolutionarily Conserved Key Regulator of Inflammation In Vivo. Curr. Biol. *31*, 875-883.e5. 10.1016/J.CUB.2020.11.014.

86. Westerfield, M. (2000). The zebrafish book. A guide for the laboratory use of zebrafish (Danio rerio) 4th ed. (Univ. of Oregon Press,).

87. Ramezani, T., Laux, D.W., Bravo, I.R., Tada, M., and Feng, Y. (2015). Live imaging of

innate immune and preneoplastic cell interactions using an inducible Gal4/UAS expression system in larval zebrafish skin. J. Vis. Exp. 10.3791/52107.

88. Myllymaki, H., Elliot, A., and Feng, Y. (2023). Wholemount Edu Staining (Zebrafish Larvae). 10.17504/PROTOCOLS.IO.N92LD9429G5B/V1.

89. Picelli, S., Faridani, O.R., Björklund, Å.K., Winberg, G., Sagasser, S., and Sandberg, R. (2014). Full-length RNA-seq from single cells using Smart-seq2. Nat. Protoc. 2013 91 *9*, 171–181. 10.1038/nprot.2014.006.

90. Young, M.D., and Behjati, S. (2020). SoupX removes ambient RNA contamination from droplet-based single-cell RNA sequencing data. Gigascience *9*. 10.1093/GIGASCIENCE/GIAA151.

91. Wolock, S.L., Lopez, R., and Klein, A.M. (2019). Scrublet: Computational Identification of Cell Doublets in Single-Cell Transcriptomic Data. Cell Syst. *8*, 281-291.e9. 10.1016/J.CELS.2018.11.005.

92. DePasquale, E.A.K., Schnell, D.J., Van Camp, P.J., Valiente-Alandí, Í., Blaxall, B.C., Grimes, H.L., Singh, H., and Salomonis, N. (2019). DoubletDecon: Deconvoluting Doublets from Single-Cell RNA-Sequencing Data. Cell Rep. *29*, 1718-1727.e8. 10.1016/J.CELREP.2019.09.082.

93. Hafemeister, C., and Satija, R. (2019). Normalization and variance stabilization of single-cell RNA-seq data using regularized negative binomial regression. Genome Biol. *20*, 1–15. 10.1186/S13059-019-1874-1/FIGURES/6.

94. Santos-Pereira, J.M., Gallardo-Fuentes, L., Neto, A., Acemel, R.D., and Tena, J.J.

(2019). Pioneer and repressive functions of p63 during zebrafish embryonic ectoderm specification. Nat. Commun. 2019 101 *10*, 1–13. 10.1038/s41467-019-11121-z.

95. Hobbs, G.A., Der, C.J., and Rossman, K.L. (2016). RAS isoforms and mutations in cancer at a glance. J. Cell Sci. *129*, 1287–1292. 10.1242/JCS.182873/260209/AM/RAS-ISOFORMS-AND-MUTATIONS-IN-CANCER-AT-A-GLANCE.

96. Hänzelmann, S., Castelo, R., and Guinney, J. (2013). GSVA: Gene set variation analysis for microarray and RNA-Seq data. BMC Bioinformatics *14*, 1–15. 10.1186/1471-2105-14-7/FIGURES/7.

97. Pearce, D.A., Nirmal, A.J., Freeman, T.C., and Sims, A.H. (2018). Continuous Biomarker Assessment by Exhaustive Survival Analysis. bioRxiv, 208660. 10.1101/208660.

Figure files:

Figure 1
Figure 2
Figure 3
Figure 4
Figure 5
Figure 6
Figure 7
Figure 8

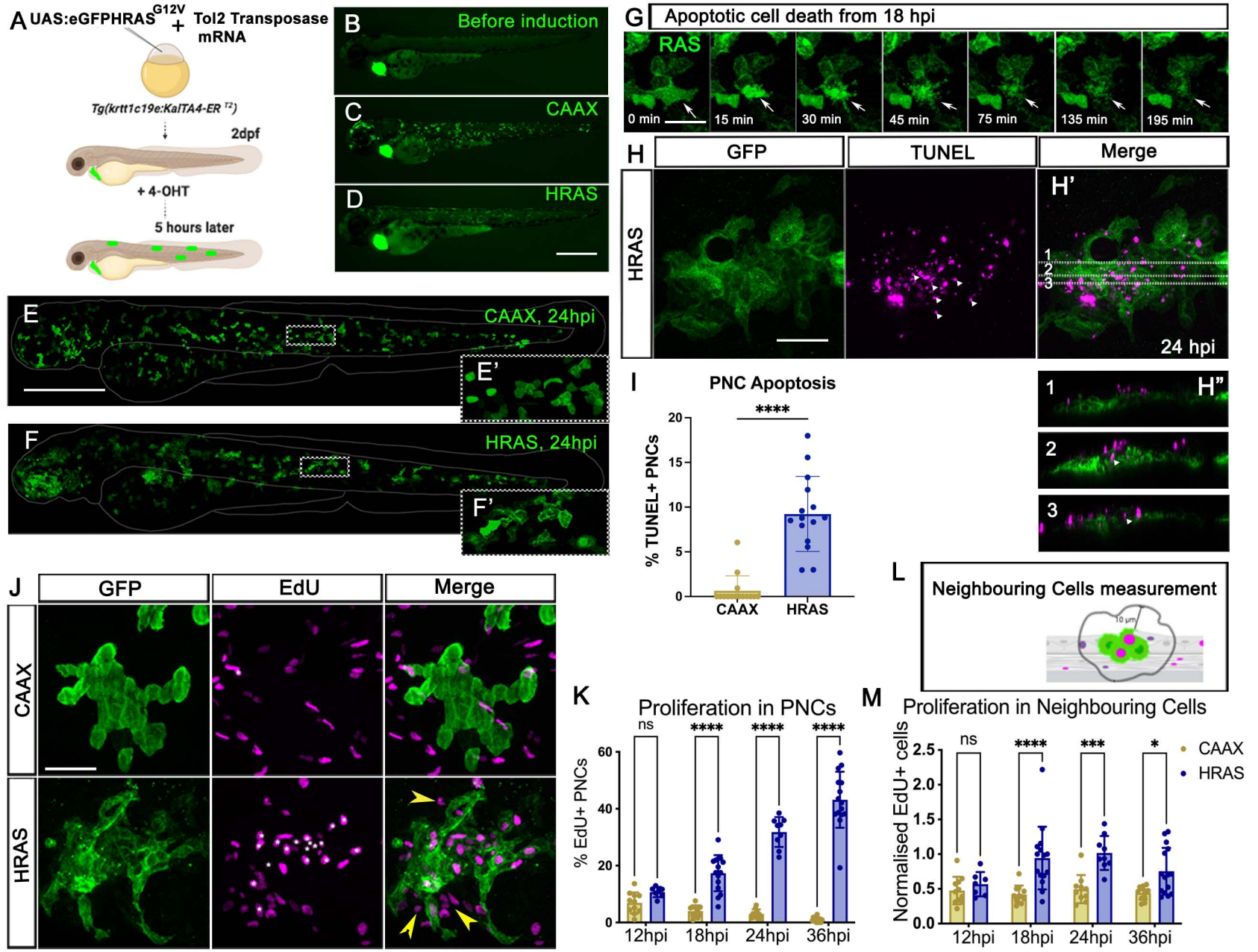
A
UAS:eGFPHRAS G12V + Tol2 Transposase mRNA
Tg(krtt1c19e:KalTA4-ER T2)
2dpf
+ 4-OHT
5 hours later
B
Before induction
C
CAAX
D
HRAS
E
CAAX, 24hpi
E'
F
HRAS, 24hpi
F'
G
Apoptotic cell death from 18 hpi
RAS
0 min
15 min
30 min
45 min
75 min
135 min
195 min
H
GFP
TUNEL
Merge
HRAS
H'
24 hpi
H"
I
PNC Apoptosis
% TUNEL+ PNCs
CAAX
HRAS
J
GFP
EdU
Merge
CAAX
HRAS
K
Proliferation in PNCs
% EdU+ PNCs
ns
12hpi
18hpi
24hpi
36hpi
L
Neighbouring Cells measurement
M
Proliferation in Neighbouring Cells
Normalised EdU+ cells
CAAX
HRAS

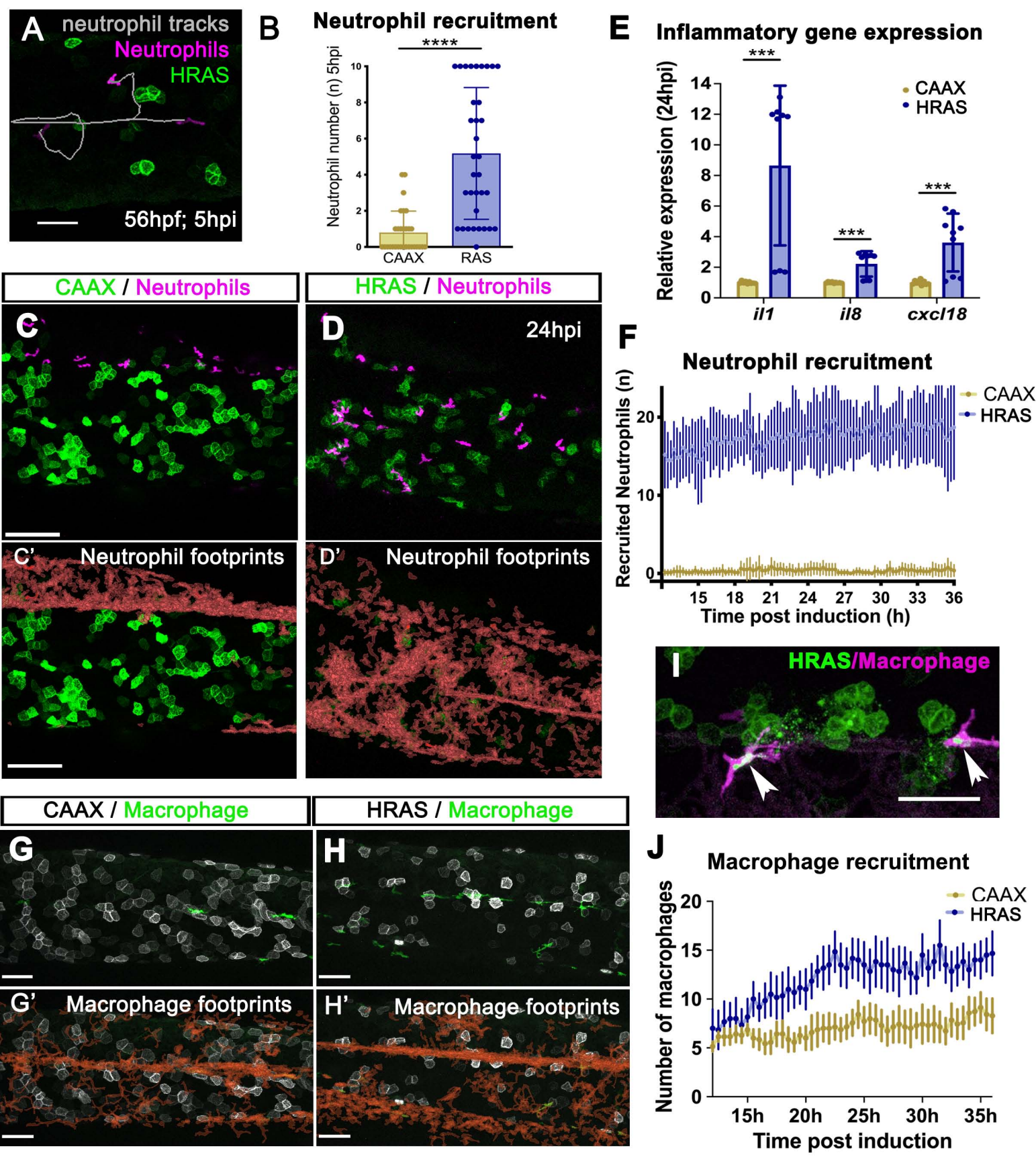
A
neutrophil tracks
Neutrophils
HRAS
56hpf; 5hpi
B
Neutrophil recruitment
****
Neutrophil number (n) 5hpi
CAAX
RAS
E
Inflammatory gene expression
***
Relative expression (24hpi)
CAAX
HRAS
il1
il8
cxcl18
CAAX / Neutrophils
HRAS / Neutrophils
C
D
24hpi
C'
Neutrophil footprints
D'
Neutrophil footprints
F
Neutrophil recruitment
Recruited Neutrophils (n)
Time post induction (h)
I
HRAS/Macrophage
CAAX / Macrophage
HRAS / Macrophage
G
H
G'
Macrophage footprints
H'
Macrophage footprints
J
Macrophage recruitment
Number of macrophages
Time post induction

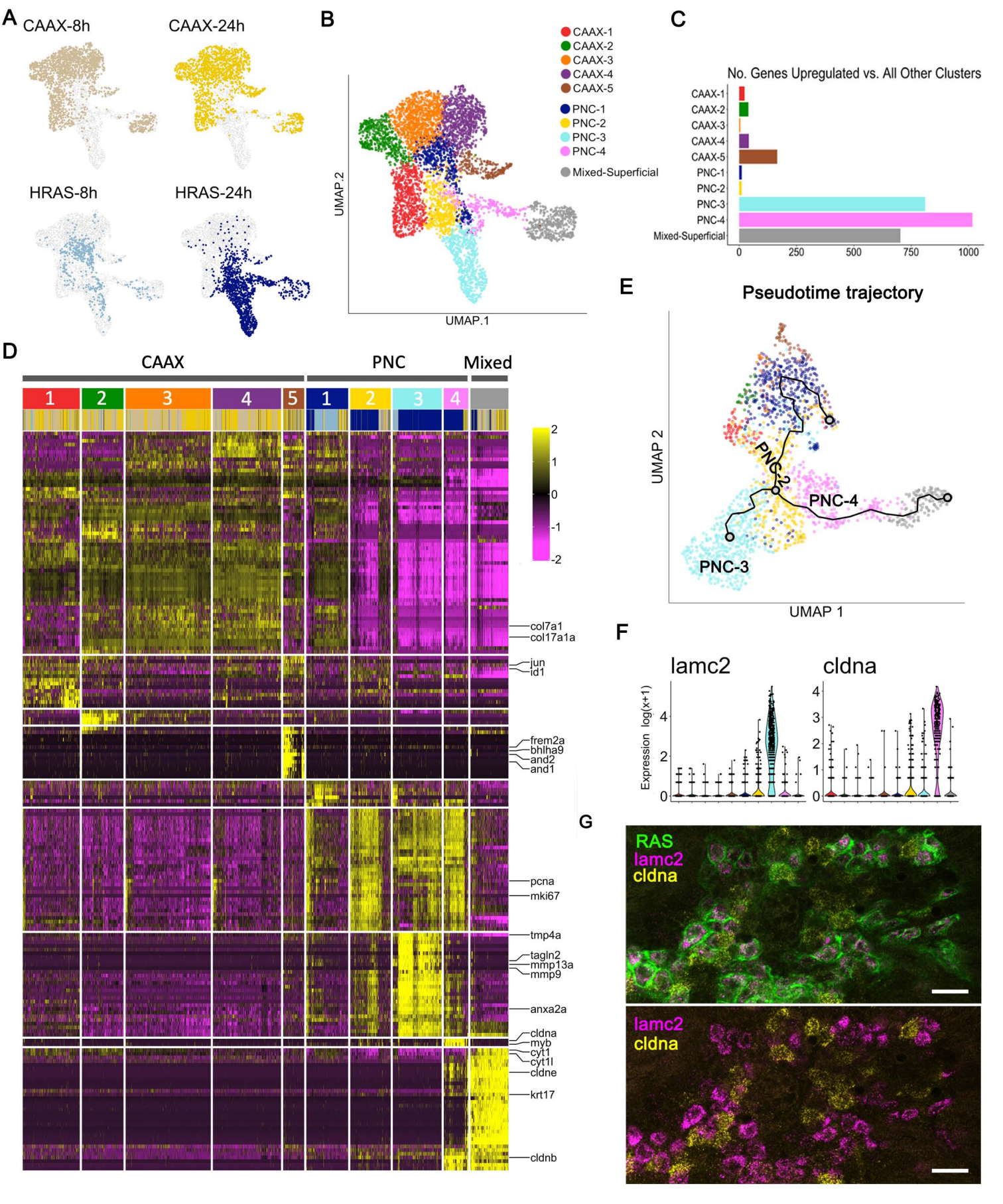
A
CAAX-8h
CAAX-24h
HRAS-8h
HRAS-24h
B
CAAX-1
CAAX-2
CAAX-3
CAAX-4
CAAX-5
PNC-1
PNC-2
PNC-3
PNC-4
Mixed-Superficial
UMAP.2
UMAP.1
C
No. Genes Upregulated vs. All Other Clusters
CAAX-1
CAAX-2
CAAX-3
CAAX-4
CAAX-5
PNC-1
PNC-2
PNC-3
PNC-4
Mixed-Superficial
0
250
500
750
1000
D
CAAX
PNC
Mixed
1
2
3
4
5
1
2
3
4
2
1
0
-1
-2
col7a1
col17a1a
jun
id1
frem2a
bhlha9
and2
and1
pcna
mki67
tmp4a
tagln2
mmp13a
mmp9
anxa2a
cldna
myb
cyt1
cyt1l
cldne
krt17
cldnb
E
Pseudotime trajectory
UMAP 2
UMAP 1
PNC-2
PNC-4
PNC-3
F
lamc2
cldna
Expression log(x+1)
G
RAS
lamc2
cldna
lamc2
cldna

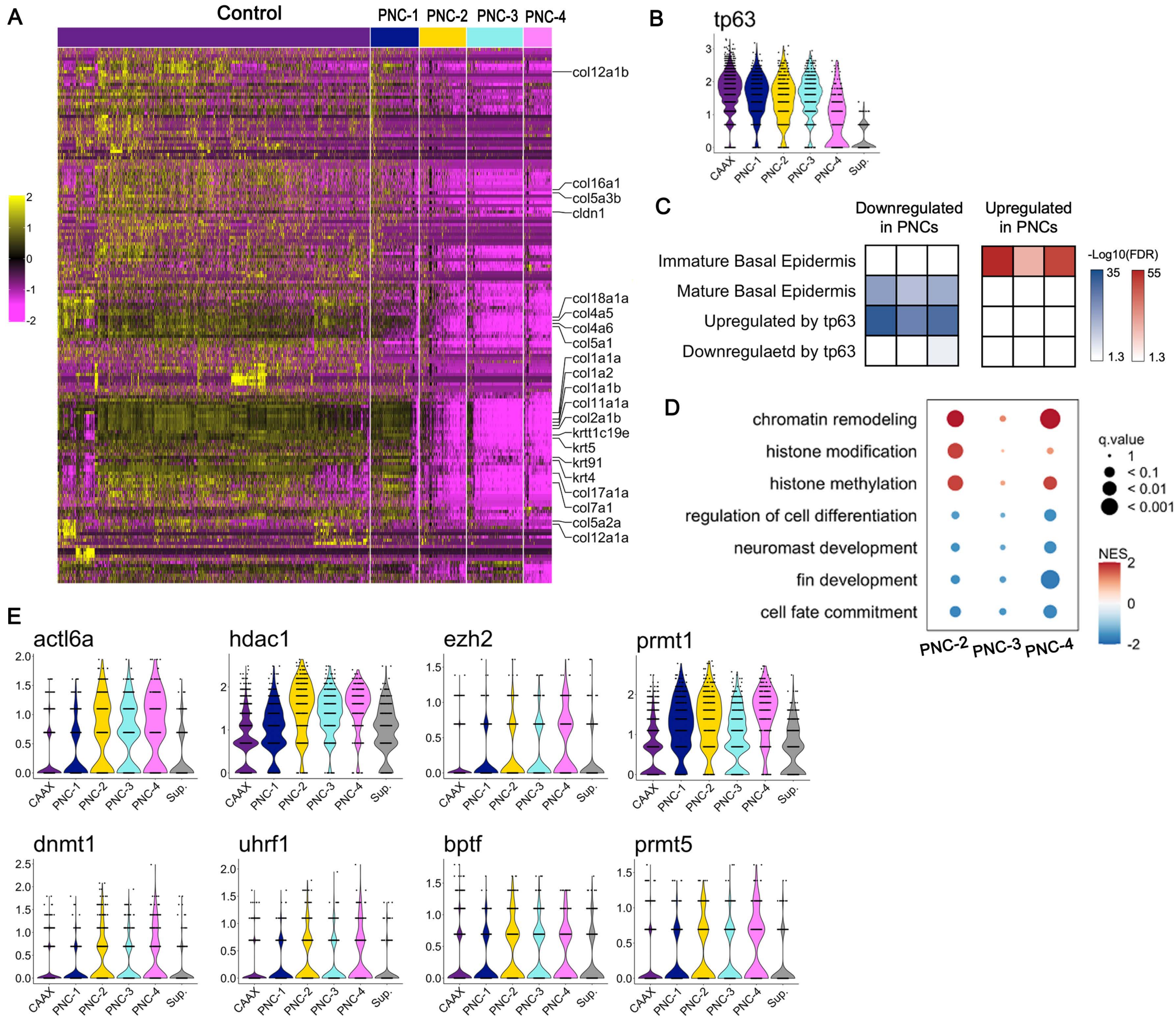
A
Control
PNC-1
PNC-2
PNC-3
PNC-4
col12a1b
col16a1
col5a3b
cldn1
col18a1a
col4a5
col4a6
col5a1
col1a1a
col1a2
col1a1b
col11a1a
col2a1b
krtt1c19e
krt5
krt91
krt4
col17a1a
col7a1
col5a2a
col12a1a
B
tp63
CAAX
PNC-1
PNC-2
PNC-3
PNC-4
Sup.
C
Downregulated in PNCs
Upregulated in PNCs
Immature Basal Epidermis
Mature Basal Epidermis
Upregulated by tp63
Downregulaetd by tp63
-Log10(FDR)
35
55
1.3
1.3
D
chromatin remodeling
histone modification
histone methylation
regulation of cell differentiation
neuromast development
fin development
cell fate commitment
PNC-2
PNC-3
PNC-4
q.value
1
< 0.1
< 0.01
< 0.001
NES
2
0
-2
E
actl6a
hdac1
ezh2
prmt1
dnmt1
uhrf1
bptf
prmt5

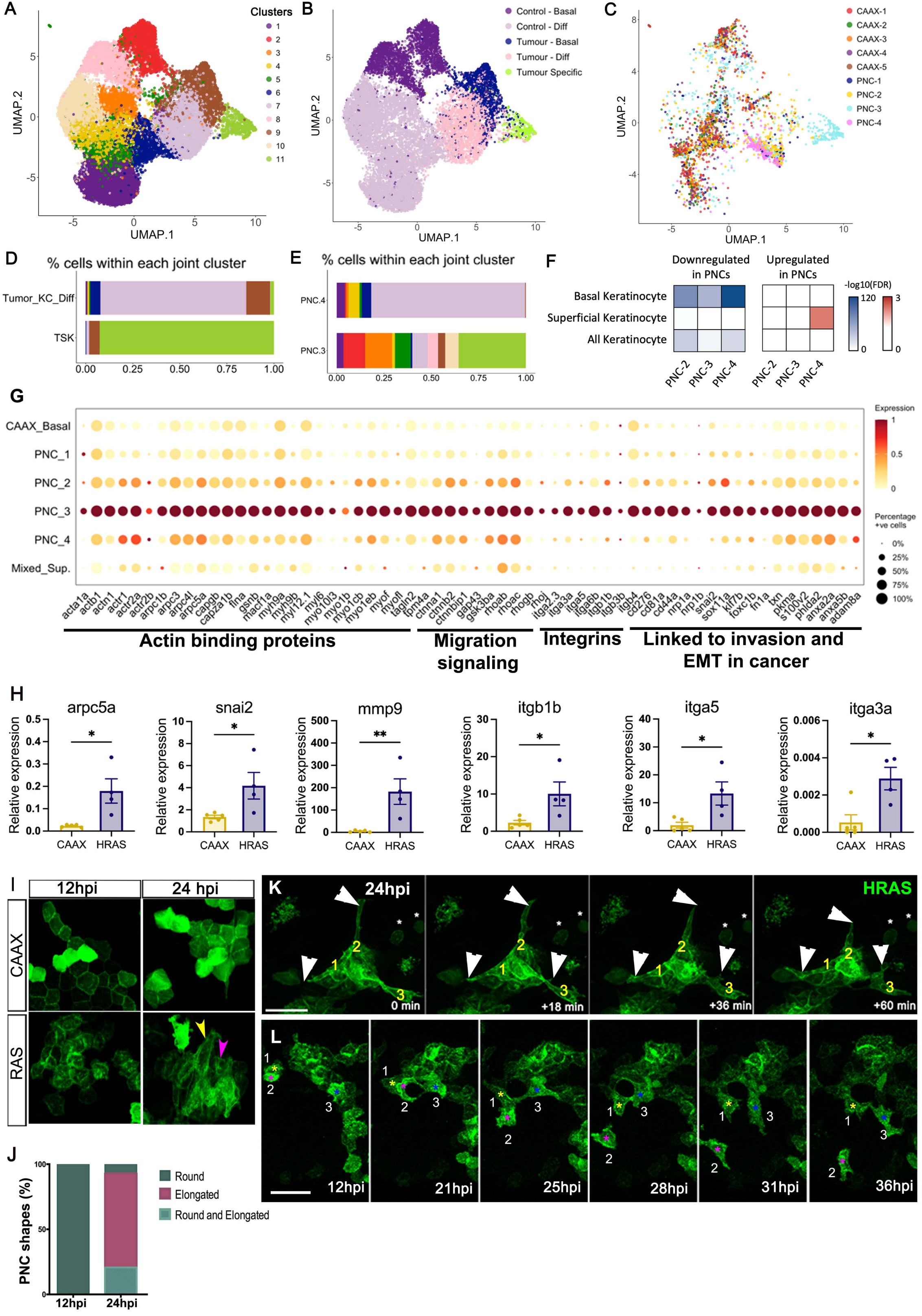
A
Clusters
1
2
3
4
5
6
7
8
9
10
11
UMAP.1
UMAP.2
B
Control - Basal
Control - Diff
Tumour - Basal
Tumour - Diff
Tumour Specific
C
CAAX-1
CAAX-2
CAAX-3
CAAX-4
CAAX-5
PNC-1
PNC-2
PNC-3
PNC-4
D
% cells within each joint cluster
Tumor_KC_Diff
TSK
E
% cells within each joint cluster
PNC.4
PNC.3
F
Downregulated in PNCs
Upregulated in PNCs
-log10(FDR)
Basal Keratinocyte
Superficial Keratinocyte
All Keratinocyte
PNC-2
PNC-3
PNC-4
G
CAAX_Basal
PNC_1
PNC_2
PNC_3
PNC_4
Mixed_Sup.
Expression
Percentage +ve cells
Actin binding proteins
Migration signaling
Integrins
Linked to invasion and EMT in cancer
H
arpc5a
snai2
mmp9
itgb1b
itga5
itga3a
Relative expression
CAAX
HRAS
I
12hpi
24 hpi
CAAX
RAS
J
PNC shapes (%)
Round
Elongated
Round and Elongated
12hpi
24hpi
K
24hpi
HRAS
0 min
+18 min
+36 min
+60 min
L
12hpi
21hpi
25hpi
28hpi
31hpi
36hpi

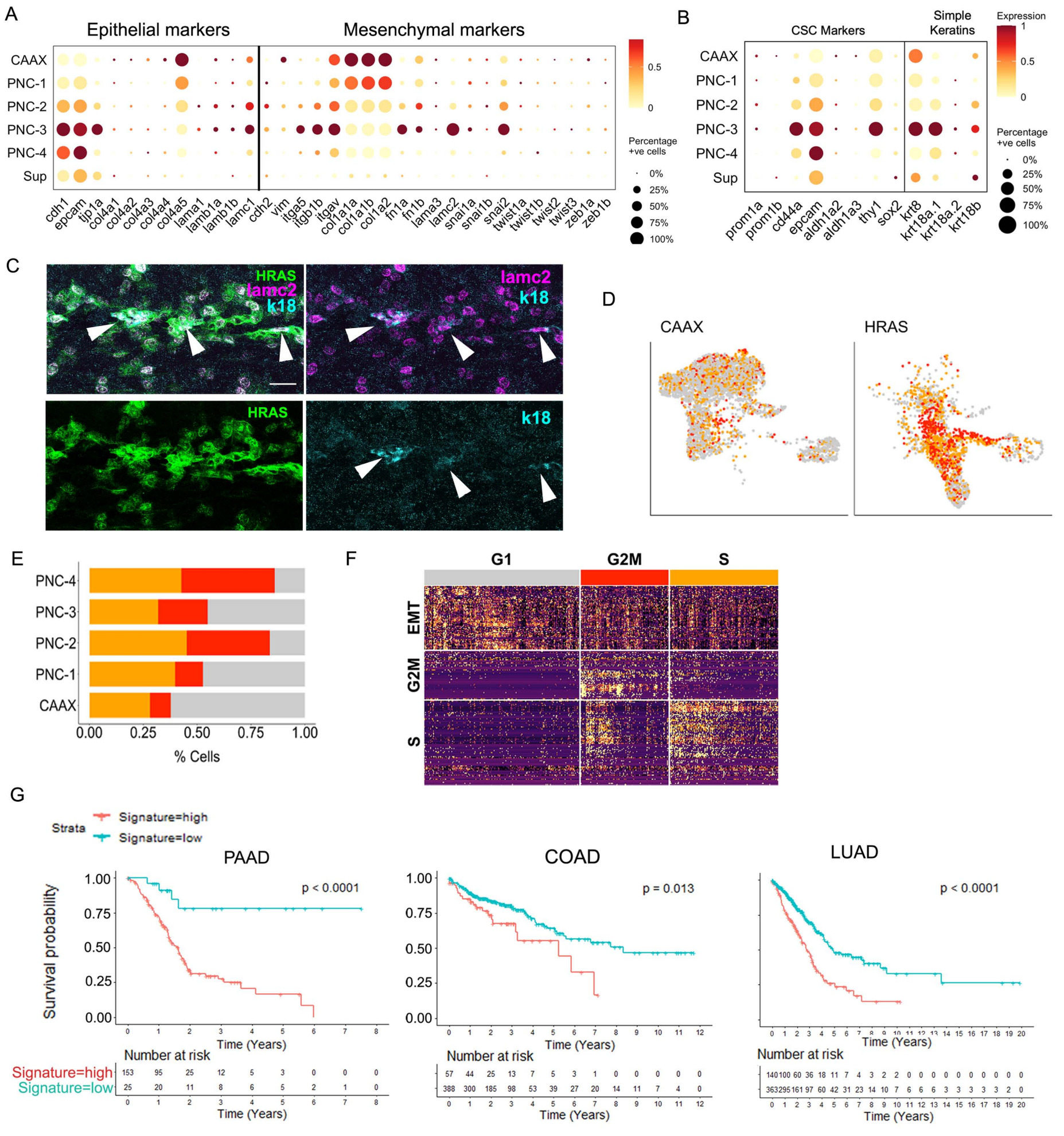
A
Epithelial markers
Mesenchymal markers
CAAX
PNC-1
PNC-2
PNC-3
PNC-4
Sup
cdh1 epcam tjp1a col4a1 col4a2 col4a3 col4a4 col4a5 lama1 lamb1a lamb1b lamc1 cdh2 vim itga5 itgb1b itgav col1a1a col1a1b col1a2 fn1a fn1b lama3 lamc2 snai1a snai1b snai2 twist1a twist1b twist2 twist3 zeb1a zeb1b
Percentage +ve cells
0% 25% 50% 75% 100%
B
CSC Markers
Simple Keratins
Expression
prom1a prom1b cd44a epcam aldh1a2 aldh1a3 thy1 sox2 krt8 krt18a.1 krt18a.2 krt18b
C
HRAS
lamc2
k18
D
CAAX
HRAS
E
% Cells
F
G1
G2M
S
EMT
G2M
S
G
Strata
Signature=high
Signature=low
PAAD
COAD
LUAD
Survival probability
p < 0.0001
p = 0.013
p < 0.0001
Time (Years)
Number at risk
Signature=high 153 95 25 12 5 3 0 0 0
Signature=low 25 20 11 8 6 5 2 1 0
57 44 25 13 7 5 3 1 0 0 0 0 0
388 300 185 98 53 39 27 20 14 11 7 4 0
140 100 60 36 18 11 7 4 3 2 2 0 0 0 0 0 0 0 0 0
363 295 161 97 60 42 31 23 14 10 7 6 6 6 3 3 3 3 3 2 0

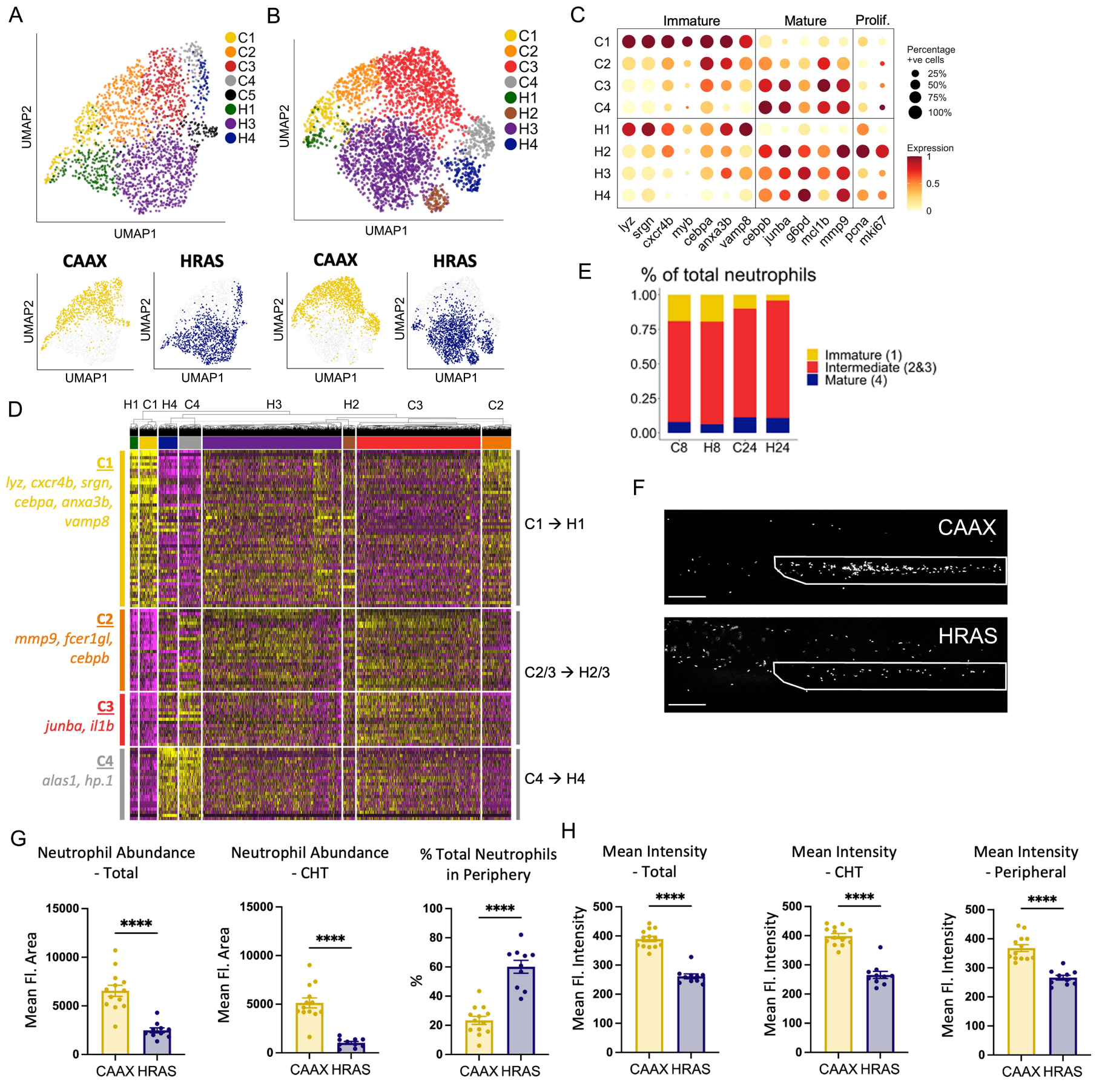
A
UMAP2
UMAP1
C1
C2
C3
C4
C5
H1
H3
H4
B
UMAP2
UMAP1
C1
C2
C3
C4
H1
H2
H3
H4
CAAX
HRAS
CAAX
HRAS
UMAP2
UMAP1
C
Immature
Mature
Prolif.
C1
C2
C3
C4
H1
H2
H3
H4
lyz
srgn
cxcr4b
myb
cebpa
anxa3b
vamp8
cebpb
junba
g6pd
mcl1b
mmp9
pcna
mki67
Percentage +ve cells
25%
50%
75%
100%
Expression
1
0.5
0
E
% of total neutrophils
1.00
0.75
0.50
0.25
0.00
C8
H8
C24
H24
Immature (1)
Intermediate (2&3)
Mature (4)
D
H1 C1 H4 C4
H3
H2
C3
C2
C1
lyz, cxcr4b, srgn, cebpa, anxa3b, vamp8
C2
mmp9, fcer1gl, cebpb
C3
junba, il1b
C4
alas1, hp.1
C1 → H1
C2/3 → H2/3
C4 → H4
F
CAAX
HRAS
G
Neutrophil Abundance - Total
Neutrophil Abundance - CHT
% Total Neutrophils in Periphery
Mean Fl. Area
%
****
CAAX
HRAS
H
Mean Intensity - Total
Mean Intensity - CHT
Mean Intensity - Peripheral
Mean Fl. Intensity
****
CAAX
HRAS

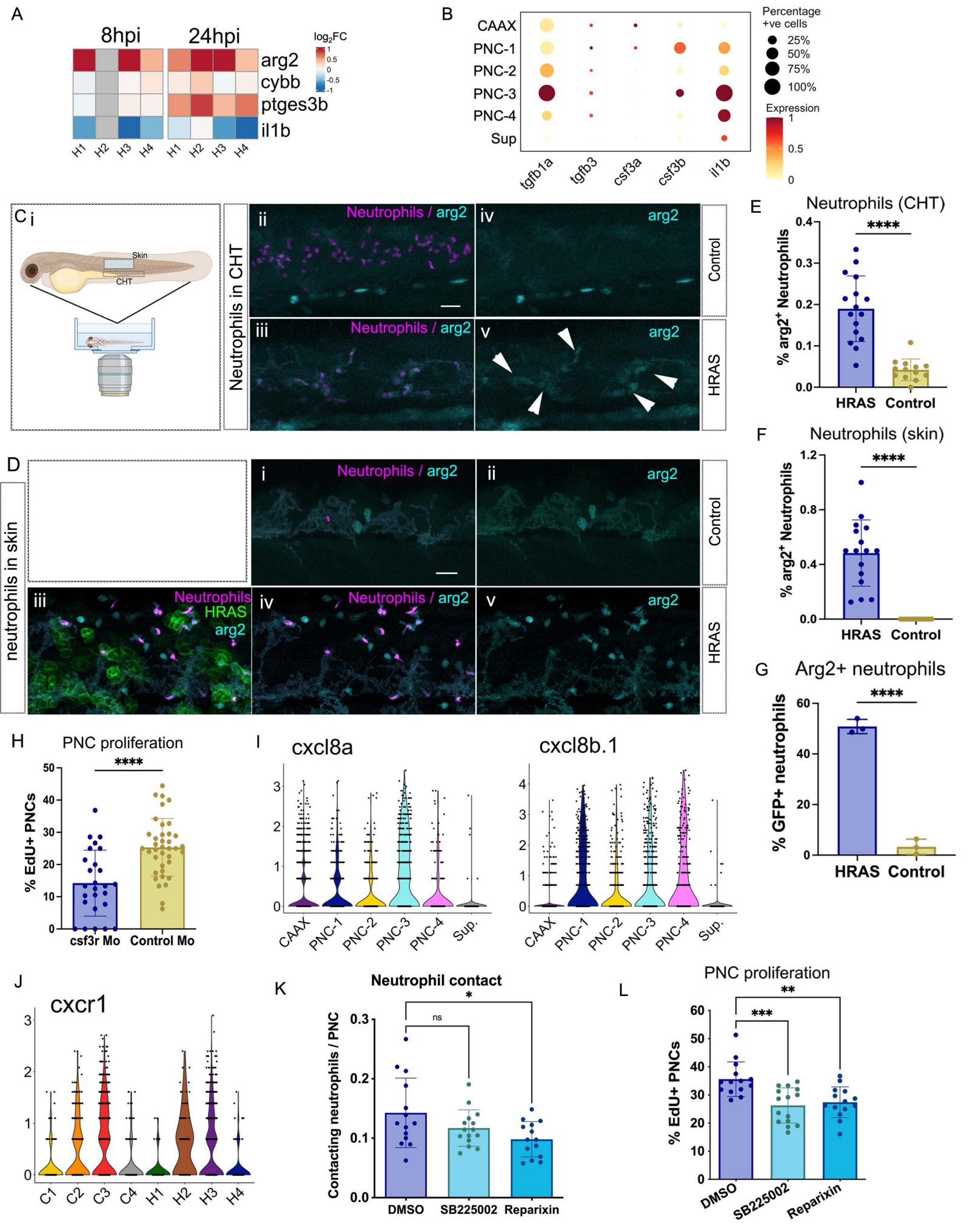
A
8hpi
24hpi
log2FC
arg2
cybb
ptges3b
il1b
H1 H2 H3 H4 H1 H2 H3 H4
B
CAAX
PNC-1
PNC-2
PNC-3
PNC-4
Sup
tgfb1a
tgfb3
csf3a
csf3b
il1b
Percentage +ve cells
25%
50%
75%
100%
Expression
C i
Skin
CHT
Neutrophils in CHT
ii Neutrophils / arg2
iv arg2
Control
iii Neutrophils / arg2
v arg2
HRAS
E
Neutrophils (CHT)
% arg2+ Neutrophils
****
HRAS Control
F
Neutrophils (skin)
% arg2+ Neutrophils
****
HRAS Control
D
neutrophils in skin
i Neutrophils / arg2
ii arg2
Control
iii Neutrophils HRAS arg2
iv Neutrophils / arg2
v arg2
HRAS
G
Arg2+ neutrophils
% GFP+ neutrophils
****
HRAS Control
H
PNC proliferation
% EdU+ PNCs
****
csf3r Mo Control Mo
I
cxcl8a
cxcl8b.1
CAAX PNC-1 PNC-2 PNC-3 PNC-4 Sup.
J
cxcr1
C1 C2 C3 C4 H1 H2 H3 H4
K
Neutrophil contact
Contacting neutrophils / PNC
ns
*
DMSO SB225002 Reparixin
L
PNC proliferation
% EdU+ PNCs
***
**
DMSO SB225002 Reparixin